

The Transcriptome Architecture of Polyomaviruses

2

3 Jason Nomburg^{1,2,3}, Wei Zou⁴, Thomas C. Frost^{1,3}, Chandreyee Datta^{5,6,7,8}, Shobha
4 Vasudevan^{5,6,7,8}, Gabriel J. Starrett⁹, Michael J. Imperiale^{4,10}, Matthew Meyerson^{1,2,11*}
5 James A. DeCaprio^{1,3,12*}

6

7 ¹Department of Medical Oncology, Dana-Farber Cancer Institute, Boston MA

⁸ ²Broad Institute of MIT and Harvard, Cambridge, MA

9 ³Harvard Program in Virology, Harvard University Graduate School of Arts and Sciences,
10 Boston, MA

11 ⁴Department of Microbiology and Immunology, University of Michigan, Ann Arbor,
12 Michigan

13 ⁵Massachusetts General Hospital Cancer Center, Harvard Medical School, 185
14 Cambridge St, CPZN4202, Boston, MA

15 ⁶Department of Medicine, Massachusetts General Hospital and Harvard Medical School,
16 Boston, MA

17 ⁷Center for Regenerative Medicine, Massachusetts General Hospital, Harvard Medical
18 School, Boston, MA

19 ⁸Harvard Stem Cell Institute, Harvard University, Cambridge, MA

20 ⁹Laboratory of Cellular Oncology, CCR, NCI, NIH, Bethesda, MD, USA

21 ¹⁰Rogel Cancer Center, Ann Arbor, MI

22 ¹¹Department of Genetics, Harvard Medical School, Boston, MA

23 ¹²Department of Medicine, Brigham and Women's Hospital, Harvard Medical School,
24 Boston, MA

25

26 *Correspondence to:

27 James A. DeCaprio

28 james_decaprio@dfci.harvard.edu

29

30 Matthew Meyerson

31 matthew_meyerson@dfci.harvard.edu

32

33 Abstract

34 Polyomaviruses (PyV) are ubiquitous pathogens that can cause devastating human
35 diseases. Due to the small size of their genomes, PyV utilize complex patterns of RNA
36 splicing to maximize their coding capacity. Despite the importance of PyV to human
37 disease, their transcriptome architecture is poorly characterized. Here, we compare
38 short- and long-read RNA sequencing data from eight human and non-human PyV. We
39 provide a detailed transcriptome atlas for BK polyomavirus (BKPyV), an important
40 human pathogen, and the prototype PyV, simian virus 40 (SV40). We identify pervasive
41 wraparound transcription in PyV, wherein transcription runs through the polyA site and
42 circles the genome multiple times. Comparative analyses identify novel, conserved
43 transcripts that increase PyV coding capacity. One of these conserved transcripts
44 encodes superT, a T antigen containing two RB-binding LxCxE motifs. We find that
45 superT-encoding transcripts are abundant in PyV-associated human cancers. Together,
46 we show that comparative transcriptomic approaches can greatly expand known
47 transcript and coding capacity in one of the simplest and most well-studied viral families.

48

49 Introduction

50 Polyomaviruses (PyV) are ubiquitous pathogens that can cause devastating human
51 diseases (Jiang et al., 2009a) including polyomavirus-associated nephropathy (PVAN),
52 hemorrhagic cystitis, and bladder cancer associated with BKPyV (Starrett et al., 2021),
53 progressive multifocal leukoencephalopathy caused by JCPyV, Merkel cell carcinoma
54 caused by Merkel cell polyomavirus (MCPyV), and dermatosis caused by human

55 polyomavirus 7 (HPyV7) (Jiang et al., 2009a; Nguyen et al., 2017). PyV have circular
56 double-stranded DNA genomes and express viral genes with distinct “early” and “late”
57 kinetics. Early and late transcripts are driven by a bi-directional central promoter, and
58 each terminate at their own polyA signal sequence located between the early and late
59 regions. The PyV early region encodes tumor or T antigens that promote cell cycle
60 progression and facilitate replication of the viral genome by host DNA polymerase. The
61 PyV late region originating from the common PyV promoter element on the opposite
62 genome strand encodes the structural proteins required for the generation of progeny
63 virions.

64

65 PyV transcripts undergo complex splicing to increase their coding capacity in the face of
66 their small ~5kb genomes. In addition to the major large T (LT) and small T (ST)
67 antigens, additional T antigen splice forms have been identified including transcripts that
68 generate truncated versions of LT (17kT, 57kT, truncT, and T' in SV40, MCPyV,
69 BKPyV, and JCPyV respectively), a “superT” antigen that contains a duplicated LxCxE
70 RB-binding motif in SV40, middle T (MT) in murine PyV (MPyV), and ALTO in MCPyV
71 (Abend et al., 2009; Carter et al., 2013; Freund et al., 1992; Kress et al., 1979; Shuda et
72 al., 2008; Smith et al., 1979; Trowbridge and Frisque, 1995; Zerrahn et al., 1993).
73 Although the diversity of late transcripts has been explored in SV40 (Good et al., 1988),
74 late transcript diversity in other PyV, including the major human pathogens, is poorly
75 characterized. To address this lack of knowledge of PyV transcription and to discover
76 unannotated biologically relevant PyV-encoded protein products, we used long- and

77 short-read RNA sequencing technologies to characterize the transcriptomes of eight
78 human and non-human PyVs.

79

80 **Results**

81 **RNA sequencing expands PyV transcript diversity.**

82 To expand known PyV transcript diversity, we conducted a series of viral infections
83 followed by total or polyA short-read Illumina RNA sequencing (short-RNAseq (total)
84 and short-RNAseq (polyA) respectively) (**Figure 1A**). We integrated this newly
85 generated data with publicly available data from infected cell culture, human skin, and
86 other settings (**Table 1**). Viruses studied include SV40, BKPyV Dunlop variant and Dik
87 (wild type, or archetype), JCPyV, MPyV, MCPyV, HPyV7, and bark scorpion
88 polyomavirus 1 (BSPyV1).

89

90 For SV40 and the BKPyV Dunlop variant, which replicate robustly in cell culture, we
91 complemented short-read sequencing with Nanopore direct RNA sequencing
92 (dRNAseq) and PacBio Single-Molecule Real-Time sequencing (SMRTseq) (**Figure**
93 **1A**), two long-read sequencing approaches for polyA RNA with distinct library
94 preparations and sequencing strategies. Resultant RNAseq reads from long- and short-
95 read sequencing strategies were mapped against the viral reference genome and
96 grouped into transcript classes based on the presence of shared introns as detailed in
97 the Methods (**Figure 1B**). For SV40, viral transcripts represented 11.6% and 8.8% of

98 transcripts in dRNAseq and SMRTseq, respectively. For BKPyV Dunlop, viral transcripts
99 represented 28.6% and 27.8% of transcripts in dRNAseq and SMRTseq, respectively.
100 The total number of viral reads is detailed in **Figure S1A**. Transcripts within the same
101 class contain the same introns but may have distinct transcript start sites (TSSs) and
102 transcript end sites (TESs). For most transcriptomes, the majority of transcripts are
103 members of the first few transcript classes (**Figure S1B**). To filter out erroneous splice
104 sites, we required that all introns present in a dRNAseq or SMRTseq read must also be
105 supported by at least 5 splice junction-spanning reads in short-RNAseq (total) data.
106 Detailed information on this transcript class strategy is present in the Methods.

107

108 Comparison of read coverage from short-RNAseq (total), dRNAseq, and SMRTseq
109 revealed that dRNAseq and SMRTseq were relatively consistent with read coverage,
110 generally reflected expected patterns of exon usage (**Figure 1C**). In contrast, the read
111 coverage of short-RNAseq (total) was less representative of expected viral exon usage
112 and may reflect noise due to the amplification of smaller RNA fragments (**Figure 1C**).

113

114 For SV40 and BKPyV Dunlop, a transcript class (consisting of transcripts with shared
115 introns) was considered a bona-fide viral transcript if it was at least 0.1% of late or early
116 transcripts in dRNAseq or SMRTseq data as described in the Methods. For SV40,
117 which has detailed splice annotations (Good et al., 1988), we found that dRNAseq and
118 SMRTseq data are largely consistent with existing annotations. However, we identified
119 five previously unannotated SV40 transcripts that were supported by both long-read

120 sequencing approaches, plus one additional previously unannotated SV40 transcript
121 class supported by SMRTseq and short-RNAseq (total) (**Figure 1D, Figure 2**).

122

123 In contrast to SV40 and despite its clinical importance, BKPyV transcripts have been
124 poorly characterized. We identified a total of 23 transcripts, 21 of which are supported
125 by both dRNAseq and SMRTseq data and only six of which were previously identified
126 (Abend et al., 2009; Seif et al., 1979) (**Figure 1E, Figure 3**). While novel BKPyV late
127 transcripts are often analogous to the characterized wraparound and non-wraparound
128 transcripts previously identified in SV40, several additional and unexpected BKPyV
129 early transcripts were identified. For example, an atypically early TSS revealed a splice
130 donor that was used to generate transcript E3 (**Figure S4**). Early transcripts including
131 E6, E9, and E11 are conserved across numerous PyV and lead to formation of novel
132 ORFs - these are described in detail below.

133

134 We generated a comprehensive atlas of SV40 and BKPyV transcripts in **Figures S3 -**
135 **S8**. Watch plots display the structure of each identified transcript, and read pileups
136 show all transcripts identified in each transcript class. The relative abundance of each
137 transcript as well as exact splice coordinates and abundance information for each
138 identified transcript is provided in **Supplementary Tables 1 and 2**. Transcripts can also
139 be explored using an interactive Google Colab notebook
140 (https://colab.research.google.com/github/jnoms/SV40_transcriptome/blob/main/bin/cola_b/PyV_exploratory.ipynb). A comprehensive analysis of all splice sites detected in short-

142 read short-RNAseq (total) and short-RNAseq (polyA) in eight PyV studied is presented
143 in **Figure S9**.

144

145 To address the possibility that distinct transcript isoforms could be preferentially
146 translated, we performed polysome profiling of SV40-infected cells coupled with
147 dRNAseq of whole-cell and polysome-associated polyadenylated RNAs (**Figure 1F**).
148 The ribosome occupancy, determined as the ratio between a transcript's normalized
149 polysome abundance and its normalized whole-cell abundance, has a mean of slightly
150 above 1 for host transcripts (**Figure S2D**). We found 11.2% of reads in the whole-cell
151 fraction and 18.7% in the polysome fraction were viral, consistent with active translation
152 of viral transcripts. For late transcripts, the relative abundance in the whole-cell fraction
153 was tightly coupled to polysome relative abundance (**Figure 1G**), indicating limited
154 preferential translation of late transcripts. In contrast to late transcripts, we found that
155 the LT:ST ratio was 1.3:1 in the polysome fraction compared to a 3.4:1 ratio of LT:ST
156 transcripts in the whole-cell fraction, indicating preferential translation of ST during
157 infection.

158

159 **Wraparound transcription is conserved across diverse PyV.**

160 Long-read sequencing revealed the existence of many late transcripts that contain
161 multiple copies of a duplicated leader exon. Leader-leader splicing is due to
162 “wraparound transcription” of PyV transcripts that failed to terminate at the late
163 polyadenylation signal and continue to circle the genome repeatedly. PyV wraparound

164 transcription has been described previously although the structure and diversity of these
165 RNA species is unknown (Adami et al., 1989; Garren et al., 2015; Luo and Carmichael,
166 1991; Reddy et al., 1978). We investigated these transcripts in dRNASeq data from
167 SV40 and BKPyV. To supplement these data, we also performed dRNASeq on MPyV-
168 infected cells. Wraparound transcription, defined by the presence of repetitive copies of
169 a shared leader sequence, was found in long-read sequencing for all three PyVs
170 (**Figure 4A, B, C**: note the presence of the leader-leader or repeated exon near the “11
171 o’clock” position in watch plots). In addition to this leader sequence repetition, there are
172 diverse forms of wraparound transcripts that contain various combinations of
173 subsequent introns and encode for distinct viral proteins (**Figure 2, 3**). While only 3.6%
174 of SV40 transcripts originate from wraparound transcription, BKPyV and MPyV have
175 markedly higher rates at 25% and 41% respectively (**Figure 4D**).

176

177 Next, we inferred the presence of wraparound transcription in diverse PyV by identifying
178 short-RNASeq (total) reads that span the leader-leader junction (**Figure 4E**). Despite the
179 limited length of these short reads, leader-leader junctions can be accurately identified
180 within a single read through analysis of junction sites (**Figure 4F**). We found evidence of
181 wraparound transcription in all eight PyV investigated here. This includes HPyV7
182 RNASeq from infected human skin and RNASeq data from a scorpion containing the
183 highly divergent Bark scorpion polyomavirus 1 (BSPyV1), indicating that wraparound
184 transcription occurs *in vivo* and is widely conserved across PyV.

185

186 **Pervasive premature polyadenylation of early transcripts in SV40, BKPyV, and**
187 **MPyV.**

188 We found that many early transcripts in SV40 and BKPyV underwent alternative
189 polyadenylation (APA) earlier than the canonical polyA site as indicated by premature
190 transcript end positions near 3 o'clock in the watch plots (**Figure S10A, B**). Early
191 transcript APA had been previously identified in MPyV, where there is a canonical polyA
192 signal sequence (AATAAA) within the LT ORF (Kamen et al., 1980b; Norbury and Fried,
193 1987). Indeed, dRNAseq identified APA of early transcripts in MPyV-infected cells
194 (**Figure S10C, D**). In contrast to MPyV, APA in SV40 and BKPyV may be driven by
195 alternative polyA signal sequences to the 5' of the APA site (ATTAAA in SV40,
196 AAGAAA or TATAAA in BKPyV). Assessment of the cumulative incidence of early
197 transcript termination shows abrupt increases in transcript termination ~1500nt
198 upstream of the canonical polyA site in all three viruses (**Figure S10D**). This APA
199 appears to be similarly abundant in LT and ST transcripts. We found that transcripts
200 with APA still contain a full polyA tail that, while shorter than the polyA tails of transcripts
201 that use the canonical polyA site, still tend to be longer than the polyA tails of host
202 transcripts (**Figure S10E, S10F, S10G, S2C**). The polyA tail length of a spike-in control
203 RNA with a known 30-adenine polyA tail was correctly estimated by dRNAseq (**Figure**
204 **S2C**). We find that transcripts containing APA can associate with polysomes (**Figure**
205 **S10H, I**), indicating that these transcripts are translated.

206

207 **Comparative analysis of short-RNAseq (total) data reveals conserved,**
208 **unannotated splice-forms that may generate variant ORFs.**

209 Next, we conducted a comparative analysis of PyV transcription from short-RNAseq
210 (total) data (**Figure S9**), with the hypothesis that data from diverse PyV could reveal
211 unannotated splice forms. This analysis led to the discovery of several unannotated but
212 conserved splicing events that have the potential to expand the coding capacity of PyV
213 (**Figure 5**).

214

215 We found that PyVs including HPyV7, MPyV, BKPyV Dunlop, and MCPyV express a
216 transcript utilizing the LT first exon donor but an acceptor within the ST ORF leading to
217 the generation of the ST2 ORF (**Figure 5A**). This splice occurs in-frame in HPyV7 and
218 BKPyV resulting in an internal deletion within ST, while in MPyV and MCPyV this splice
219 lands out of frame and results in the addition of novel C-terminal amino acids. The ST2
220 splice is highly abundant in HPyV7 representing over 20% of spliced early transcripts
221 from HPyV7-infected human skin. ST2-encoding transcripts were detected in BKPyV
222 dRNAseq and SMRTseq data (transcript E6).

223

224 MPyV encodes MT in addition to the LT and ST antigens common with other PyV.
225 MPyV MT is generated from a splicing event that connects the ST ORF with an ORF in
226 the alternative frame of the LT second exon. To our surprise, we found that BKPyV
227 expresses low levels of a similar transcript containing a splice that connects the ST
228 ORF with an MT-like ORF likewise in an alternative frame of the LT second exon
229 (**Figure 5B**). This MT transcript was also detected in BKPyV dRNAseq and SMRTseq
230 data (transcript E9).

231

232 JCPyV encodes two VP1 variants, VP1Xs, that consist of the N-terminal region of VP1
233 with novel C-termini that make up as much as 30% of late spliced transcripts in JCPyV
234 (**Figure 5C**) and have been recently identified and validated by an independent group
235 (Saribas et al., 2018). We found that VP1X-encoding transcripts were also produced by
236 MCPyV, SV40, BKPyV, and MPyV, albeit at a lower abundance than in JCPyV. Except
237 for one JCPyV VP1X-encoding splice, these transcripts were generated from splicing of
238 wraparound transcripts that run through the late polyA signal sequence.

239

240 **SuperT, a T antigen containing two RB-binding motifs, is present in multiple PyV**
241 **and in PyV-associated human cancers.**

242 Studies in SV40-transformed cells previously identified a superT antigen with higher
243 molecular weight than LT, containing a duplicated region with two copies of the LxCxE
244 RB-binding motif (Eul and Patzel, 2013). We found that a superT-specific splice was
245 present in SV40, BKPyV (Dik and Dunlop variants), JCPyV, and MCPyV during viral
246 infection (**Figure 5D**). The superT-specific splice originates from a splice donor
247 canonically associated with a conserved truncated LT antigen (17kT in SV40, truncT in
248 BKPyV, 57kT in MCPyV, and T' in JCPyV), but uses the LT second exon acceptor
249 available due to wraparound transcription. We find evidence of superT in the dRNAseq
250 and SMRTseq data for SV40 and BKPyV Dunlop infections (transcripts E4 and E11
251 respectively). Western blot with an antibody reactive to LT in BKPyV Dik-infected cells
252 revealed a band with slightly higher molecular weight than LT that is consistent with

253 superT (**Figure 5F**). BKPyV Dik mutant M1, designed to remove ST by replacing the LT
254 intron with an intron from the plasmid pCI (**Figure 5E**), also generated a superT band of
255 expected size. BKPyV Dik mutant M2 was generated by removing the LT intron and
256 adding the pCI intron just 5' of the LT first exon. Should the truncT donor be used to
257 generate superT in this mutant, the only available acceptor is before the LT 1st exon,
258 which would result in the formation of an aberrantly larger superT due to the inclusion of
259 a second copy of the LT first exon (**Figure 5E**). short-RNAseq (polyA) analysis of cells
260 infected with BKPyV Dik WT, M1, or M2 show junctions consistent with this model
261 (**Figure S11**), and western blot revealed that the superT band in M2 is shifted to a
262 higher molecular weight (**Figure 5F**). Together, these data indicate that superT is
263 generated by BKPyV Dik during viral infection.

264

265 SuperT was initially identified as an unexplained higher-molecular weight T antigen
266 present in many SV40-transformed cell lines (Kress et al., 1979; Smith et al., 1979).
267 While superT can be generated during viral infection because of wraparound
268 transcription, in SV40-transformed cells it would be possible to yield pre-mRNAs that
269 can be spliced to form superT should the virus be integrated in tandem copies (**Figure**
270 **6A**). Indeed, we previously observed that MCPyV integration events in Merkel cell
271 carcinoma (MCC) often lead to partial duplications of the viral genome and result in the
272 tandem insertion of multiple copies of viral early genes (Starrett et al., 2020).
273 Furthermore, the duplicated region in superT includes the RB-binding LxCxE motif,
274 raising the possibility that superT can function as a potent oncogene. We therefore
275 asked if there is evidence of superT in PyV-associated human cancers.

276

277 To address this question, we first analyzed short-RNAseq (total) data from five BKPyV-
278 associated bladder cancers (Starrett et al., 2021). To our surprise, we found that short-
279 RNAseq (total) data from two replicates of one BKPyV-associated bladder cancer
280 contained a higher abundance of superT-specific splice than even the LT- or ST-specific
281 splices, suggesting that a large fraction of “LT” in this tumor is superT (**Figure 6B**). We
282 next analyzed short-RNAseq (polyA) data from a series of 30 MCPyV-positive MCCs
283 and found evidence of superT in six cases (**Figure 6B**). Notably, the total number of
284 viral reads in some MCPyV-positive but superT-null tumors was very low, leaving open
285 the possibility that sequencing depth was insufficient to identify the superT splice in
286 additional tumors. Using PCR and sanger sequencing, we confirmed the presence of
287 the superT splice in MCC tumor J45_440 (**Figure S12A**).

288

289 We hypothesized that superT may be generated by cis-splicing due to concatemeric
290 integration of multiple copies of the etiologic PyV in these tumors (**Figure 6A**). To
291 address this hypothesis, we investigated three MCCs (J45_440, J17_296, J11_285) for
292 which we possess short-read whole genome sequencing data. From J11_285, we were
293 able to assemble the entire integration site, showing that MCPyV is integrated in a
294 manner that could allow cis-splicing to generate superT (**Figure S12B**). For J45_440,
295 we assembled a single viral block integrated in chromosome 7 (**Figure S12C**). We
296 found that 1) there are likely 2 copies of the viral genome, and 2) the 5' viral integration
297 site appears to fall on chromosome 7 “after” the 3' viral integration site, observations
298 consistent with the existence of two copies of the viral genome in tandem separated by

299 a small segment of host DNA at this integration site. For J17_296, from the assembly,
300 we could infer three distinct segments of viral DNA with integration sites closely spaced
301 within chromosome 2 (**Figure S12D**), indicating a complex integration pattern. The
302 longer block contains two copies of the early region and can likely support superT
303 generation through cis-splicing. The LT ORF of MCPyV is often truncated by premature
304 stop codons or deletions in MCC. We found that a stop codon in J17_296 likely
305 prevents expression of superT, but no stop codons occur before the superT splice in
306 J45_440 or J11_285 (**Figure S12E**). Together, these data indicate that viral integration
307 sites often could support cis-splicing to generate superT.

308 Two recent studies have found evidence of circular RNAs (circRNAs) that may be
309 generated by MCPyV in MCC and may support the translation of ALTO (Abere et al.,
310 2020; Yang et al., 2021). Of note, the major circRNA splice is equivalent to our
311 proposed MCPyV superT splice - a short-RNAseq read spanning the proposed circRNA
312 junction cannot be differentiated from a read spanning the superT junction. However,
313 the MCC RNAseq samples in which we found superT are short-RNAseq (polyA), which
314 should select against the potential circRNA due to its lack of a polyA tail. Furthermore,
315 we detect the superT splice in short-RNAseq (polyA) of SV40 and BKPyV Dunlop
316 infections in cell culture (**Figure S9**), although at around ~2/3 of its relative abundance
317 in short-RNAseq (total). Finally, we identify full-length superT transcripts in dRNAseq
318 data, which is highly unlikely to sequence circRNA since it is not polyadenylated. This
319 leaves open the possibility that some superT-like splice in short-RNAseq (total) from
320 viral infection originates from circRNA but suggests that most are from linear transcripts
321 that contain a polyA tail.

322

323 **Discussion**

324 Here, we show that leveraging multiple long- and short-read RNA sequencing
325 approaches across 8 polyomaviruses has allowed us to greatly expand known transcript
326 diversity of this viral family. Short read RNAseq has limited capacity to characterize
327 transcriptome diversity because only a small fraction of reads span splice junctions, and
328 these junctions often cannot be phased with other junctions or to the transcript start and
329 end sites. Integrating long-read sequencing has allowed sequencing of entire
330 transcripts, including phasing of splice sites and transcript start and end positions.

331 Recent studies have leveraged long read sequencing to shed light on exceptional
332 complexity in the transcriptomes of diverse RNA and DNA viruses (Balázs et al., 2017;
333 Depledge et al., 2019; Garalde et al., 2018; Keller et al., 2018; Kim et al., 2020;
334 Nomburg et al., 2020; Price et al., 2020). We have expanded these studies to show that
335 a comparative approach within a viral family can identify conserved transcripts that
336 extend viral coding capacity.

337

338 Historically, studies of PyV transcripts were limited by the sensitivity and resolution of
339 northern blots, or by the read length of short read sequencing. Despite these limitations,
340 studies in the 70's and 80's were able to cumulatively characterize several SV40 late
341 transcripts, including one containing leader-leader splicing (Ghosh et al., 1978; Good et
342 al., 1988; Reddy et al., 1978). In contrast to SV40, the architecture of BKPyV late
343 transcripts is poorly characterized - prior to this work, the two major classes of late

344 transcripts (“16S” and “19S”, reflecting transcript size based on gradient sedimentation
345 properties) were the primary late transcript classifications (Seif et al., 1979). Only
346 recently did a study provide some evidence for leader-leader splicing in BKPyV (Zou et
347 al., 2020). While the late transcripts of most PyV are thought to encode the canonical
348 late viral proteins, a recent study in JCPyV identified two splice events that lead to the
349 generation of novel proteins containing the N-terminal region of VP1 - one of which was
350 validated through western blot (Saribas et al., 2018). We found that these transcripts
351 (deemed “VP1X”) are highly expressed in JCPyV but are also expressed at lower level
352 in BKPyV, MPyV, MCPyV, and SV40.

353

354 Leader-leader splicing is known to be highly prevalent in MPyV, where as many as 12
355 leader exons have been observed on a single RNA (Kamen et al., 1980a; Legon et al.,
356 1979; Treisman, 1980) - in our data, we have identified over 15 leader exons in a single
357 transcript. Furthermore, leader-leader splicing is required for stable accumulation of
358 MPyV late transcripts, dependent on length but not nucleotide composition of the leader
359 (Adami et al., 1989). Despite these observations, the exact structure, diversity, and
360 conservation of wraparound transcripts was not understood. Here, we found that leader-
361 leader splicing and wraparound transcription occurs in all PyV studied, including in the
362 divergent Bark scorpion polyomavirus 1, and found that the prevalence of leader-leader
363 splicing varies significantly between PyV. It is possible that this variation reflects
364 differences in the strength of the late polyA signals of these PyV. We found a large
365 diversity of wraparound transcripts containing variable numbers of the leader sequence
366 and diverse patterns of subsequent exon usage.

367

368 While late and early transcripts are thought to primarily end at the canonical late or early
369 polyadenylation sites, studies previously observed APA of early transcripts in MPyV
370 (Kamen et al., 1980b; Norbury and Fried, 1987). Here, we likewise identify pervasive
371 APA of early SV40 and BKPyV Dunlop transcripts and find that SV40 early transcripts
372 with APA can associate with polysomes and are likely translated. In addition, polysome
373 profiling revealed that SV40 transcripts are higher abundance in polysome-associated
374 RNAs than in whole-cell RNA populations, indicating preferential translation of SV40
375 transcripts. The relative abundance of individual late viral transcripts in the polysome
376 closely reflected their whole-cell abundance - conversely, ST transcripts were
377 preferentially translated compared to LT transcripts. The mechanism driving this
378 difference needs further study, as these transcripts differ only by a minor difference in
379 splice donor usage.

380

381 In addition to the major early transcripts encoding LT and ST, other early transcripts
382 have been identified in some PyV. MPyV encodes MT, generated by a splice
383 connecting the ST ORF and an ORF overprinted with LT second exon. MT is a primary
384 oncogene in MPyV and was thought to be largely restricted to rodent PyVs (Gottlieb and
385 Villarreal, 2001). We found that BKPyV generates a MT-like ORF through splicing
386 connecting ST and an ORF similarly overprinted with the LT second exon, showing that
387 non-rodent PyVs may be capable of expressing MT-like ORFs. In addition, MPyV also
388 encodes a tinyT antigen consisting largely of the LT first exon, resulting from a splice
389 connecting the LT first exon donor and MT acceptor (Riley et al., 1997). We identified a

390 novel T antigen, ST2, that is generated from a splice from the LT first exon donor to a
391 splice acceptor within the ST ORF. This transcript is highly expressed in HPyV7 and
392 present at lower levels in BKPyV, MPyV, and MCPyV. Many PyV encode a truncated
393 variant of LT - this includes SV40 17kT, BKPyV truncT, MCPyV 57kT and JCPyV T'
394 proteins (Abend et al., 2009; Shuda et al., 2008; Trowbridge and Frisque, 1995; Zerrahn
395 et al., 1993). These transcripts contain a canonical LT splice and a subsequent splice
396 that removes a large portion of the LT ORF.

397

398 We found that the same secondary splice sites responsible for truncated LT variants
399 can be used to generate superT. superT was initially observed in many SV40-
400 transformed cell lines (Kress et al., 1979; Smith et al., 1979) - in a similar manner, we
401 find that concatemeric integration of BKPyV and MCPyV in human cancers can facilitate
402 the generation of superT. We also find that superT is generated in lytic infections of
403 SV40, BKPyV, MCPyV and JCPyV. Eul and colleagues have published several studies
404 proposing that SV40 superT can be generated by trans-splicing between two separate
405 pre-mRNAs in the context of artificial expression constructs encoding the SV40 early
406 region (20, 31, 32). However, we find that in MCC tumors that generate superT and for
407 which we can assemble the viral integration site, the viral genome is likely integrated in
408 tandem in a way that could facilitate the cis-splicing of pre-mRNA that spans multiple
409 genome copies. Thus, while we cannot rule out trans-splicing from these data, we
410 believe cis-splicing is more likely. Future studies are necessary to understand the
411 biology of superT including its oncogenic potential and ability to bind multiple RB
412 molecules. Finally, efforts should be taken to understand if superT is expressed by PyV

413 and contributes to disease in other contexts, such as by BKPyV in PVAN or JCPyV in
414 PML.

415

416 We show that complex, uncharacterized splicing events are used by PyV to expand
417 their protein coding capacity. Future work is necessary to understand the biological
418 function of these transcripts and proteins. It is possible that unannotated splicing we
419 identify here could be differentially abundant in other biological contexts, so it will be
420 important to investigate PyV splicing in other infection contexts and human diseases.
421 Future transcriptome analyses that integrate long and short reads from multiple viruses
422 may have utility to expand characterized transcript and coding capacity in other viral
423 families.

424

425 Conclusions

426 We provide a comprehensive transcriptome atlas for the prototype PyV SV40, as well
427 as the critically important human pathogen BKPyV. Comparative analyses of PyV
428 transcriptomes reveals conserved splice events that may expand PyV coding capacity.
429 We find that superT, a transcript generated by SV40, BKPyV, JCPyV, and MCPyV that
430 encodes a T antigen containing two RB-binding LxCxE domains, is present in several
431 PyV-associated human cancers. Together, these data expand our understanding of PyV
432 transcriptomes and uncover unannotated PyV-encoded proteins of potential relevance
433 to human disease.

434

435

436 **Materials and Methods**

437 **Data and code availability.**

438 All code used in this project can be found at the zenodo and github links below. The
439 zenodo repository also contains all processed data necessary to reproduce all analyses
440 and figures. The main processing steps used to process RNAseq data are present as
441 nextflow pipelines which call modular bash and python scripts.

442 Zenodo: <https://doi.org/10.5281/zenodo.5593468>

443 Github: https://github.com/jnoms/SV40_transcriptome

444

445 Furthermore, a series of interactive Google Colab notebooks can download all
446 processed data from Zenodo and completely reproduce all analyses and non-schematic
447 primary figures. The colab documents are stored on github at
448 https://github.com/jnoms/SV40_transcriptome/tree/main/bin/colab. Direct links to the
449 Google Colab documents are as follows:

450 Figure 1:

451 https://colab.research.google.com/github/jnoms/SV40_transcriptome/blob/main/bin/cola
452 [b/](https://colab.research.google.com/github/jnoms/SV40_transcriptome/blob/main/bin/cola)[Figure1.ipynb](https://colab.research.google.com/github/jnoms/SV40_transcriptome/blob/main/bin/cola)

453 Figure 4:

454 https://colab.research.google.com/github/jnoms/SV40_transcriptome/blob/main/bin/cola_b/Figure4.ipynb

456 Figure 6:

457 https://colab.research.google.com/github/jnoms/SV40_transcriptome/blob/main/bin/cola_b/Figure6.ipynb

459

460 A Google Colab notebook is available for interactive investigation of all SV40 and
461 BKPyV viral transcript classes, and does not require computational skills to use:

462 https://colab.research.google.com/github/jnoms/SV40_transcriptome/blob/main/bin/cola_b/PyV_exploratory.ipynb

464

465 All raw RNA sequencing data are available at the NCBI sequence read archive at
466 accession **XXXXXX**.

467

468 **Datasets**

469 Information on all samples and viruses (excluding tumors) can be found in **Table 1**.

Table 1

Virus	Sequencing Type	Origin (Accession)	MOI / Timepoint	Host

SV40	dRNAseq (two replicates)	Generated here	MOI 1 / 48hpi	<i>C. Sabaeus</i>
SV40	SMRTseq	Generated here	MOI 1 / 48hpi	<i>C. Sabaeus</i>
SV40 (polysome input/whole-cell)	dRNAseq	Generated here	MOI 1 / 44hpi	<i>C. Sabaeus</i>
SV40 (polysome)	dRNAseq	Generated here	MOI 1 / 44hpi	<i>C. Sabaeus</i>
SV40	Short-RNAseq (total)	Generated here	MOI 1 / 48hpi	<i>C. Sabaeus</i>
SV40	short-RNAseq (polyA)	Generated here	MOI 1 / 48hpi	<i>C. Sabaeus</i>
BKPyV (Dunlop)	dRNAseq	Generated here	MOI 0.5 / 3dpi	Human
BKPyV (Dunlop)	SMRTseq	Generated here	MOI 0.5 / 3dpi	Human
BKPyV (Dunlop)	Short-RNAseq (total)	Generated here	MOI 0.5 / 3dpi	Human
BKPyV (Dunlop)	short-RNAseq (polyA)	Generated here	MOI 0.5 / 3dpi	Human
BKPyV (Dik) WT	Short-RNAseq (total)	Generated here	MOI 1 / 5dpi	Human
BKPyV (Dik) WT	Short-RNAseq (polyA)	Generated here	MOI 1 / 5dpi	Human
BKPyV (Dik) M1	Short-RNAseq (polyA)	Generated here	MOI 1 / 5dpi	Human

BKPyV (Dik) M2	Short-RNAseq (polyA)	Generated here	MOI 1 / 5dpi	Human
MPyV	dRNAseq	Generated here	Unknown / 28hpi	Mouse
MPyV	Short-RNAseq (total)	Garren et al. (Garren et al., 2015) (SRR2043214)	MOI 50 / 36hpi	Mouse
JCPyV	Short-RNAseq (total)	Assetta et al. (Assetta et al., 2016) (SRR9967610)	Unknown / 9dpi	Human
MCPyV (Synthetic genome)	short-RNAseq (polyA)	Theiss et al. (Theiss et al., 2015) (EBI: ERS760222)	200ng viral DNA / Unknown	Human
HPyV7	Short-RNAseq (total)	Rosenstein et al. (Rosenstein et al., 2021) (SRR11488976, SRR11488977)	From infected human skin	Human
BSPyV1	Short-RNAseq (total)	Identified by Schmidlin et al. (Schmidlin et al., 2021) (SRR5958578)	From whole scorpion	<i>C. sculpturatus</i>

470

471 **Tumor samples**

472 The BKPyV-associated bladder cancer is sample TBC03 that has been described

473 (Starrett et al., 2021). This sample is stranded, short-RNAseq (total).

474

475 Merkel cell carcinoma samples: Sections of tissue were isolated from patient-derived

476 tumor biopsies and suspended in RNAlater (Thermo Fischer) until further processing.

477 RNA and DNA was extracted from each section via the AllPrep DNA/RNA kit (Qiagen).
478 Isolated RNA and DNA were each sequenced (PE150) on the NovaSeq 6000 platform
479 (Illumina) for a depth of 50 M reads or 60x genomic coverage per sample, respectively
480 (Novogene). RNAseq data are unstranded, short-RNAseq (polyA).

481

482 **SV40 infection and RNA extraction**

483 BSC40 cells (ATCC CRL-2761) were seeded on 150mm dishes at 5.37×10^6 cells per
484 plate - about 70% confluence. After waiting 4 hours for the cells to adhere, cells were
485 infected with SV40 at MOI 1 as previously described (Tremblay et al., 2001) with slight
486 modification. In brief, maintenance media was removed, and each 150mm dish was
487 inoculated with 6mL of virus stock diluted in DMEM + 2% FBS. Infection was allowed to
488 proceed at 37°C, 5% CO₂ for one hour, with the plates rocked every 15 minutes to
489 ensure adequate coverage of the solution over the cell monolayer. At the end of this
490 period, DMEM + 2% FBS was added to a final volume of 25mL per 150mm dish. Each
491 dish was then incubated at 37°C, 5% CO₂ for 48 hours. RNA was extracted using the
492 QIAGEN RNeasy Mini Plus Kit (QIAGEN 74134). This total RNA was then subjected to
493 Nanopore direct RNA sequencing and Illumina total- and polyA-RNA sequencing as
494 described below.

495

496 **BKPyV infection and RNA extraction**

497 Archetype and rearranged BKPyV (Dik and Dunlop, respectively) were purified and
498 titrated as described (Jiang et al., 2009b). RPTE-hTERT cells (Zhao and Imperiale,

499 2019) were plated in 6-well plate and prechilled for 15 min at 4°C and infected with Dik
500 or Dunlop at a MOI of 1 and 0.5 fluorescence-forming unit (FFU)/cell, respectively. The
501 cells were incubated at 4°C for 1 h with gentle shaking every 15 min. The virus was
502 removed and fresh REGM medium was added to the cells. Dik and Dunlop infected
503 cells were collected at 120 hpi and 96 hpi, respectively. Total RNA was extracted using
504 the Direct-zol RNA MiniPrep kit (ZYMO Research, USA). This total RNA was then
505 subjected to Nanopore direct RNA sequencing and Illumina total- and polyA-RNA
506 sequencing as described below.

507

508 **MPyV infection and RNA extraction**

509 C57 mouse embryo fibroblasts (ATCC SCRC-1008) were plated on a 150mm dish at
510 40% confluence. After several hours of growth, the typical DMEM + 10% FBS media
511 was replaced with serum free DMEM. The next day, the crude viral stock was thawed at
512 37°C, incubated at 45°C for 20 minutes to facilitate the final liberation of virus into the
513 supernatant, and cell debris removed from the viral stock with centrifugation. The
514 prepared virus stock was then diluted 1:10 with an absorption buffer consisting of HBSS
515 with 10mM HEPES, 1% FBS, at pH 5.6. Media was removed from the target cells, and
516 6mL of diluted virus in absorption buffer was added. Infection was allowed to proceed at
517 37°C, 5% CO₂ for one hour, with the plates rocked every 15 minutes to ensure
518 adequate coverage of the solution over the cell monolayer. At the end of this period, the
519 absorption buffer was removed and DMEM + 2% FBS was added to a final volume of
520 25mL per 150mm dish. Cells were inoculated for 28 hours at 37°C, 5% CO₂, after which
521 RNA was extracted using TRIzol (ThermoFisher 15596026) according to the

522 manufacturer's instructions. This total RNA was then subjected to Nanopore direct RNA
523 sequencing as described below.

524

525 The virus stock used here was kindly provided by the lab of Robert Garcea. This virus
526 stock (viral strain NG59RA) was a crude supernatant from MPyV-infected cells originally
527 generated by the lab of Thomas Benjamin on 02/08/2011 and was of unknown titer.
528 This stock was subjected to a total of three freeze-thaw cycles before use.

529

530 **SV40 polysome profiling**

531 BSC40 cells were plated on 4 150mm dishes at 60% confluence. After waiting 4 hours
532 for the cells to adhere, cells were infected with SV40 at MOI 1 as reported above. At 44
533 hours post infection cell culture media was replaced with media containing 100ug/mL
534 cycloheximide and incubated for 5 minutes. Plates were placed on ice, media
535 discarded, and cells were scraped into PBS containing 100ug/mL cycloheximide. Cells
536 were spun down, the PBS discarded, and cells were lysed in a lysis buffer containing
537 10mM Tris (pH 8), 100mM KCl, 10mM MgCl₂, 2mM DTT, 1% Triton X100, 100ug/mL
538 cycloheximide, and 1unit/uL SUPERase RNase inhibitor (Thermo AM2694). Lysates
539 were incubated on ice for 20 minutes with intermittent tapping, and then spun at
540 10,000g for 10 minutes at 4°C. The supernatant was loaded onto a 10-55% sucrose
541 gradient followed by ultracentrifugation (Beckman Coulter Optima XPN-100
542 ultracentrifuge) at 32,500 × rpm at 4 °C for 80 minutes in the SW41 rotor. Gradients
543 were prepared with a gradient mixer and pump. Samples were separated by density

544 gradient fractionation system (Biocomp Piston gradient fractionator IP). RNA was
545 extracted from reserved input (“whole-cell”) lysate, as well as the polysome fraction
546 using TRIzol. Equal volumes of each fraction containing heavy polysomes (>2) was
547 pooled prior to extraction (Lee et al., 2020).

548

549 **Western blotting**

550 Infection of wildtype Dik and two Dik mutants in RPTE-hTERT cells was performed as
551 mentioned above. Protein samples were harvested in E1A buffer with protease and
552 phosphatase inhibitors, electrophoresed, transferred, and probed with large tumor
553 antigen antibody (pAb416) as previously described (Zhao and Imperiale, 2019).

554 **RNA sequencing**

555 The concentration of total RNA was determined using the Qubit Fluorometer with the
556 Qubit RNA HS Assay Kit (ThermoFisher Q32852). RNA quality was then assessed on
557 an Agilent Bioanalyzer and the RNA 6000 Pico Kit (Agilent 5067-1513). PolyA RNA was
558 isolated using the NEBNext Poly(A) mRNA Magnetic Isolation Module (NEB E7490S)
559 with an input of 5ug of total RNA - for SV40 and BKPyV Dunlop, up to 8 total reactions
560 were used to yield sufficient polyA RNA (500ng) for subsequent protocols. In the case of
561 MPyV, due to limited amounts of total RNA, three reactions were used to yield roughly
562 100ng of polyA RNA. PolyA RNA concentration was determined again using the Qubit
563 RNA HS Assay Kit (ThermoFisher Q32852). PolyA RNA was then concentrated to 9uL
564 using a centriVap.

565

566 500ng of polyA RNA (or, in the case of MPyV, 100ng) in 9uL was then processed using
567 the Nanopore Direct RNA sequencing kit (SQK-RNA002). Resultant libraries were
568 sequenced for up to 24 hours on a MinION using an R9.4.1 flow cell.

569

570 In the case of polysome profiling: extracted RNA from the input and polysomes were
571 separately subjected to 5 reactions each of the NEBNext Poly(A) mRNA Magnetic
572 Isolation Module using 5ug RNA input per reaction. All resultant polyA RNA was then
573 processed using the Nanopore Direct RNA sequencing kit (SQK-RNA002). Resultant
574 libraries were sequenced for up to 24 hours on a MinION-Mk1C using an R9.4.1 flow
575 cell.

576

577 Illumina total RNA sequencing and polyA RNA sequencing of SV40-, BKPyV Dunlop-,
578 and BKPyV Dik-infected cells was conducted by Novogene Corporation Inc. The QC for
579 the RNA samples was performed using Qubit and Bioanalyzer instruments. Libraries
580 were then prepared using NEBNext Ultra II with RiboZero Plus kit (for short-RNAseq
581 (total)) and NEBNext Ultra II with PolyA Selection kit (for short-RNAseq (polyA)). Both
582 library approaches are strand-specific. Library quality and concentration was assessed
583 with Labchip and qPCR. Libraries were sequenced on NovaSeq6000 using PE150
584 sequencing.

585

586 PacBio SMRT sequencing of SV40 and BKPyV Dunlop was conducted by the Georgia
587 Genomics and Bioinformatics Core. Each sample was subjected to IsoSeq library

588 preparation and sequenced on an individual 8M SMRT cell for 26 hours on a Sequel-II
589 machine.

590

591 **Initial Sequence Processing**

592 Raw Nanopore dRNAseq reads from standard SV40, BKPyV Dunlop, and MPyV
593 infections were basecalled with Guppy version 4.2.2 with the following command:
594 guppy_basecaller -i fast5 -s basecalled --flowcell FLO-MIN106 --kit SQK-RNA002 -r --
595 trim_strategy rna --reverse_sequence true --u_substitution true --
596 cpu_threads_per_caller 10

597

598 Raw Nanopore dRNAseq reads from polysome profiling of SV40 transcripts were
599 basecalled on a MinION-Mk1C using MinKNOW version 21.02.2.

600

601 PacBio SMRTseq subreads were processed using ccs (version 6.0.0). Full-length,
602 nonchimeric reads were then generated using the lima (version 2.0.0) and Isoseq3
603 (version 3.4.0) packages provided by PacBio.

604

605 Stranded Illumina short-RNAseq (total) and short-RNAseq (polyA) reads were
606 processed in the following way: Files containing read 1 (R1) and read 2 (R2) were
607 trimmed and adapters removed using Trim Galore! (Krueger, 2016). Next, reads in R1
608 files were reverse complemented to orient the reads correctly relative to the transcript of

609 origin, and all read headers in the R1 and R2 files were labeled with “_1” or “_2”
610 respectively. The R1 and R2 files were then concatenated. This Illumina processing
611 pipeline is available in process_illumina.nf.

612

613 The MCC tumor RNAseq assessed in this manuscript were short-RNAseq (polyA) that
614 were NOT stranded. This means that the strand of origin of each read is unknown. To
615 address this uncertainty, the complement AND reverse complement of both R1 and R2
616 were concatenated into the final FASTQ file. As described below in the section
617 “Processing of short-read short-RNAseq (total) and short-RNAseq (polyA) span files”,
618 future processing kept the most-likely alignment strand for each read.

619

620 **Sequence Alignment and Processing**

621 Most long-read sequencing data and Illumina sequencing data were aligned to the
622 appropriate viral genome using Minimap2 (Li, 2018). The exceptions are the short-
623 RNAseq (total) JCPyV data from Assetta et al. (Assetta et al., 2016) and the HPyV7
624 data from Rosenstein et al. (Rosenstein et al., 2021) - these samples contained
625 sequencing reads of 101bp or shorter and were instead mapped with STAR (Dobin et
626 al., 2013). All non-primary alignments were discarded. Sequence alignments in BAM
627 format were then converted to BED using bedtools (Quinlan and Hall, 2010). Here,
628 bedtools considers any Minimap2- or STAR-called intron (“N” cigar flag) as an intron to
629 split alignment segments. Parameters for alignment and bed conversion can be found in
630 minimap2.sh and star.sh.

631

632 To capture transcripts that originate from a pre-mRNA that circled the viral genome
633 more than once, and therefore contain repetitive sequences, all alignments were
634 conducted against concatenated copies of the viral genome. In the case of short-read
635 short-RNAseq (total) and short-RNAseq (polyA), the reference consisted of two
636 concatenated copies of the viral genome. For long-read dRNAseq and SMRTseq, the
637 reference consisted of twenty concatenated copies of the viral genome.

638

639 Because the references consisted of multiple copies of the same viral genome, mapped
640 reads were assigned to a random copy of the genome. Therefore, all reads in resultant
641 BED files were “slid” such that they started in the first genome copy of the reference
642 using bed_slide.WRAPAROUND_reads.py.

643

644 All reference genomes can be found in resources/ref directory of the associated github
645 repository. All references used contain the PyV late region at the start/5' end of the
646 reference on the “+” or sense strand, with the early region on the antisense or “-” strand.
647 The concatenated references are based on the following reference genomes collected
648 from NCBI, with any modifications listed:

649 - SV40: NC_001669.1. The first 100 nucleotides were moved to the end of the
650 sequence.
651 - BKPyV: KP412983.1
652 - JCPyV: NC_001699.1

653 - MPyV: NC_001515.2. The sequence was reverse-complemented to orient the
654 late region towards the start of the reference.
655 - MCPyV: NC_010277.2
656 - HPyV7: NC_014407.1
657 - BSPyV1: LN846618.1

658

659 Next, a span file was generated from each slid BED file using bed_to_span.py. This
660 script splits each read into “spans”, where each span is an exon or an intron with all
661 positions relative to the viral genome. The introns are defined by the Minimap2- or
662 STAR-called introns (“N” cigar flag) as mentioned above. All regions between the start
663 and end of the reads that are not introns were called as distinct exons. Transcripts were
664 clustered into transcript classes based on introns as discussed below. A “tidy” output
665 span file was then generated that contains the name, strand, and transcript class of a
666 given read, with separate lines for the start and end of each span (e.g., exon or intron)
667 within the sequencing read.

668

669 **Alignment of repetitive regions**

670 Reads that originate from a transcript that circles the genome more than once can be
671 detected because there is one or more repetitive regions within the read. Alignment
672 against multi-copy reference genomes (20 copies in the case of dRNAseq and
673 SMRTseq) as described above sufficiently captured most of these transcripts, with
674 some exceptions. First, BKPyV SMRTseq data had a poor alignment rate of the leader

675 exon in late WA transcripts - this means that WA transcripts are underrepresented in the
676 BKPyV SMRTseq data. Second, alignment of superT and superT* transcripts from
677 SMRTseq and dRNAseq data was generally poor, with the repetitive region often failing
678 to map via Minimap2. Potential superT and superT* reads in dRNAseq and SMRTseq
679 data were identified through assessment of BAM files following mapping. Early reads
680 that contain a CIGAR flag showing an insertion of 100 bases or more were flagged, and
681 up to 50 of these transcripts were manually investigated through online BLASTN
682 (Johnson et al., 2008) against the viral reference genome. Reads supporting superT in
683 SV40 dRNAseq data, superT* in SV40 SMRTseq data, and superT in BKPyV SMRTseq
684 data were initially missing from Minimap2 alignments but were identified via this
685 approach. One transcript of each type was then repaired upon data import to R such
686 that these transcripts are represented in downstream visualizations - these actions are
687 clearly marked in UTILS_import_data.R. Thus, superT and superT* in SMRTseq and
688 dRNAseq data are underrepresented in abundance plots (**Figure S3D, S4D**) and read
689 pileups (**Figure S6, S8**) compared to their actual abundance in the cell due to these
690 alignment challenges.

691

692 **Generation of transcript classes**

693 Transcript classes were generated during processing of BED files using
694 bed_to_span.py. Each transcript class consists of sequencing reads that contain the
695 same combination of introns. The transcript class number is based on the abundance of
696 transcripts within a transcript class - e.g., transcript class 1 contains more transcripts
697 than transcript class 2, and so on. Transcript class generation is similar for both long-

698 and short-read sequencing data, although short reads usually (but not always) tend to
699 contain a maximum of one intron. Notably, transcript class assignment is independent of
700 the transcript start and end positions, meaning that there can be heterogeneity of
701 transcript start and end positions within a transcript class. For all SMRTseq and
702 dRNAseq data, for a transcript class to be generated all introns contained within the
703 transcript class were required to be supported by at least 5 junction-spanning reads
704 within a short-RNAseq (total) dataset. For SV40 and BKPyV Dunlop SMRTseq and
705 dRNAseq data, the short-RNAseq (total) data was generated from RNA from the same
706 extraction. SV40 dRNAseq replicate 2 was corrected with the short-RNAseq (total) data
707 from the first SV40 replicate. For the MPyV dRNAseq data, short-RNAseq (total) data
708 from Garren et al. was used. If a transcript contained an intron that was not supported
709 by at least 5 junction-spanning reads in the Illumina dataset, it was discarded. We opted
710 to use this filtering strategy rather than implementing long-read correction because
711 correction algorithms were unable to cope with wraparound transcripts.

712

713 There were limited circumstances where dRNAseq or SMRTseq transcript classes were
714 removed manually during processing - this occurred to four transcript classes that made
715 it through filtering. In these circumstances, alignments were deemed to be artifactual
716 due to Minimap2 alignment errors. These instances are clearly programmatically
717 marked in UTILS_import_data.R with specific rationale for each action.

718

719 **Splice coordinate system**

720 All splice or intron positions marked in any figure or table of this manuscript are **0-**
721 **indexed positions of the intron.** To convert these coordinates to the 1-
722 indexed/absolute position of the intron on the viral genome, add 1 to the intron start
723 position. For example, for the intron 276-1600, viral genome nucleotide # 277 is the first
724 nucleotide within the intron, and viral genome nucleotide # 1600 is the last nucleotide
725 within the intron.

726

727 **Processing of short-RNAseq (total) and short-RNAseq (polyA) span files**

728 The majority of the short-read RNAseq data investigated here used a strand-specific
729 sequencing strategy (except for the MCC tumor RNAseq). With this strategy, the strand
730 of origin for the transcript yielding each read is known, and a read can be correctly
731 assigned to the sense (“+” / late) or antisense (“-” / early) strand. However, a fraction of
732 transcripts can be inaccurately stranded due to artifacts during library preparation.

733 When there were many more late reads than early reads in a short-read dataset, a
734 prohibitive fraction of “early” reads would be reads from late transcripts that were
735 incorrectly stranded due to this artifact. To address this issue, short reads that aligned
736 to the + strand were required to either start or end within the late region (defined as the
737 first ½ of the genome), and short-reads that aligned to the - strand were required to
738 either start or end within the early region (defined as the second ½ of the genome).

739

740 **Transcript identification**

741 For **Figure 1** and all supplementary figures, a SV40 or BKPyV transcript was identified
742 and assigned a transcript ID if it was at least 0.1% of early or late strands in dRNAseq
743 or SMRTseq data with one exception - SV40 transcript L8 had been previously
744 identified and was kept despite being at only 0.06% abundance. Existing transcript
745 names, where available, were taken from relevant studies (Abend et al., 2009; Good et
746 al., 1988; Seif et al., 1979; Zerrahn et al., 1993). This assignment occurred from the
747 span files, meaning that all sequencing reads in question were previously required to
748 contain introns that were supported by at least 5 short-RNAseq (total) junction-spanning
749 reads. For SV40, for which there were two dRNAseq replicates, identification of a
750 sequencing read at 0.1% or greater in just one replicate was sufficient.

751

752 Transcript IDs (e.g., E1, E2, E3..., L1, L2, L3,...) consist of the kinetic class (E: Early, or
753 L: Late) of the identified transcript followed by an integer value in ascending order of
754 abundance. This abundance value was calculated by ordering the transcripts in order of
755 the maximum observed relative abundance in dRNAseq or SMRTseq data.

756

757 Of note, the relative abundance of transcripts between dRNAseq and SMRTseq data is
758 skewed by distinct read-length biases between the two approaches. The dRNAseq
759 approach has a 3' bias and a bias towards shorter transcripts, while SMRTseq library
760 preparation resulted in preferential sequencing of transcripts closer to ~2500bp in
761 length. Resultant differences in the length of aligned reads can be seen in **Figure S1C**.
762 The TSS distribution of SV40 late transcripts varies between transcript classes, while

763 the late TSS distribution tends to be similar across transcript classes in BKPyV (**Figure**
764 **S2A**).

765

766 **Calculation of sequencing coverage**

767 To determine the sequencing coverage for each sample (as in **Figure 1C**), BAM files
768 from alignment were “slid” such that all transcripts must start in the first genome copy of
769 the reference using `bam_slide.WRAPAROUND_reads.py`, in a similar manner as the beds
770 were slid as described above. Forward and reverse strand reads were split, and the
771 depth was calculated using the command ``samtools depth -aa -d0`` separately for
772 forward and reverse reads. These processing steps are present in `bam_coverage.nf`.
773 During plotting, the coverage for each strand was normalized to the maximum coverage
774 at any position (e.g., the maximum coverage of the late and early strands was set to 1).

775

776 **Watch plots**

777 Each panel of a watch plot represents information for a single transcript class. The
778 center “arms” of these plots are histograms detailing the distribution of start (blue) and
779 end (red) positions for the transcripts within the transcript class. These histograms are
780 normalized to the highest abundance position. The outer ring of each watch plot shows
781 the viral ORF map. Each inner grey ring indicates the number of genomes spanned - all
782 transcripts are displayed moving outwards from the center. Red segments indicate the
783 **exons** of each transcript class. The first exon starts on the most-inner grey ring at the
784 most common transcript start site for the transcript class, and the last exon ends on the

785 most-outer grey ring at the most common transcript end site for the transcript class. The
786 3' end of the transcript is indicated by the red arrow at the end of the last exon. Thus,
787 the transcripts spiral outwards from the center in the direction of the red arrow. **Figure 4**
788 contains a schematic key describing watch plots.

789

790 **Read pileup plots**

791 Each square/rectangular panel of a read pileup plot shows the reads present in a single
792 transcript class. The arrows at the top of each panel indicate the viral ORF map, with
793 dashed lines indicating the end of each genome copy. Next, the lines indicate
794 histograms of the transcript start (blue) and end (red) sites for the transcripts within the
795 transcript class. Below the x-axis, each row indicates a single sequencing read. The
796 spans in red indicate the exons inferred from a sequencing read, while the spans in pink
797 indicate the introns/splice junctions. Sometimes the distribution of transcript end
798 positions for a transcript class can be obscured by the thickness of the transcript lines -
799 the histograms should always be consulted to assess abundance.

800

801 For SV40 dRNAseq watch and pileups: There were two SV40 dRNAseq replicates.
802 Watch plots and read pileups are based on replicate 1, although missing transcripts that
803 were identified in replicate 2 but not 1 were also plotted.

804

805 **Short-read intron plots (Figure S9, S11)**

806 In these plots, lines indicate specific introns. The upper and lower horizontal arrows
807 indicate the viral ORF map - often, these ORF maps will indicate two concatenated viral
808 reference genomes. The circles above or below each ORF map indicate the percentage
809 of early or late introns that fall at each genome position. Early introns and percentages
810 are colored red, while late introns and percentages are colored blue.

811

812 **polyA tail length**

813 polyA tail length was determined from dRNAseq data using the `polya` command of
814 Nanopolish (Loman et al., 2015). To determine the polyA distribution of host transcripts,
815 sequencing reads were aligned to the human GRCh38 (for BKPyV samples), C.
816 *Sabaeus* (for SV40 samples), or mouse (for MPyV) cDNA transcriptomes downloaded
817 from ensembl. Only reads with a Nanopolish QC tag of “PASS” were considered for
818 downstream polyA tail length analyses.

819

820 The dRNAseq library preparation included the addition of the “RNA Control Standard”
821 (RCS), which is a synthetic RNA based on yeast ENO2 containing a 30-adenine polyA
822 tail. dRNAseq samples were mapped against ENO2 to assess the polyA tail length
823 distribution of this control.

824

825 The cumulative incidence of transcript termination (**Figure S10D**) was calculated by
826 determining, for each early read, how far the read's transcript end site is from the
827 canonical polyA site position for each virus.

828

829 **Polysome profiling analysis**

830 To determine the ribosome occupancy of host genes, dRNAseq reads were aligned to
831 the *C. Sabaeus* cDNA transcriptome downloaded from ensembl. The number of reads
832 mapped to each transcript was extracted with `samtools idxstats`. Transcripts were
833 filtered to include only those with at least 10 reads in both polysome and input fractions.
834 The normalized abundance of each transcript in each fraction was defined as (# of
835 mapped reads)/(total number of virus and host mapped reads). Ribosome occupancy of
836 each transcript was determined as (normalized abundance in polysome)/(normalized
837 abundance in whole-cell), where a value of >1 indicates preferential translation.

838

839 Ribosome occupancy of individual viral transcripts could not be calculated because of
840 increased rates of transcript truncation in the polysome fraction compared to the whole-
841 cell fraction. This was indicated by a nearly doubled proportion of unspliced reads with
842 premature 5' ends in the polysome fraction compared to the whole-cell fraction, and
843 likely indicates transcript degradation during sucrose centrifugation or fraction collection.
844 Because viral transcripts are mostly identical and vary largely at a 5' splice site,
845 elevated transcript truncation decreased the observed abundance of individual viral

846 transcripts in the polysome fraction and make ribosome occupancy calculations for
847 individual viral transcripts unreliable.

848

849 **MCC440 superT PCR and sanger sequencing**

850 Anchored poly-dT primers (Life Technologies) were used for specific reverse-
851 transcription of full-length mRNA into cDNA. Primers were designed to uniquely amplify
852 the super-LT junction through exploitation of repetitive sequences. Primer sequences
853 were as follows (5' -> 3'); Forward: CTGGACTGGGAGTCTGAAGC, Reverse:
854 ACCCCTCCTCCATTCTCAAGA. Q5 polymerase (NEB) with standard reaction
855 conditions was used for amplification.

856

857 **Generation of integrated PyV structures and viral variant calling**

858 Tumor WGS was aligned against a fusion reference genome containing hg38 and
859 Merkel cell polyomavirus (NC_010277) using bowtie2 with default parameters.
860 Integrated virus assembly graphs and annotations were generated using Oncovirus
861 tools (https://github.com/gstarrett/oncovirus_tools). Assembly graphs were then
862 manually interpreted to create linear integration structures for PyV-associated MCC.

863

864 Point mutations were called in the PyV genomes using lofreq with default parameters
865 (<https://csb5.github.io/lofreq/>) (PMID: 23066108). Lofreq output was functionally
866 annotated with SnpEff (<http://pcingola.github.io/SnpEff/>) (PMID: 22728672) using the

867 relevant GenBank gene annotations for the above genomes. Variants were plotted out
868 in R with the ggplot2 package.

869

870

871 **List of abbreviations**

872 APA - Alternative polyadenylation

873 BKPyV - BK Polyomavirus

874 BSPyV1 - Bark scorpion polyomavirus 1

875 dRNAseq - Nanopore direct RNA sequencing

876 HPyV7 - Human polyomavirus 7

877 JCPyV - JC Polyomavirus

878 LT - Large T antigen

879 MCC - Merkel cell carcinoma

880 MCPyV - Merkel cell polyomavirus

881 MPyV - Murine polyomavirus

882 MT - Middle T antigen

883 ORF - Open reading frame

884 SMRTseq - PacBio SMRT sequencing

885 ST - Small T antigen
886 SV40 - Simian virus 40
887 TES - Transcript end site
888 TSS - Transcript start site
889 PVAN - Polyomavirus-associated nephropathy
890 PyV - Polyomavirus
891
892

893 **Declarations**

894 **Competing interests**
895 M.M. receives research support from Bayer, Janssen, Ono; consults for Bayer, Interline,
896 Isabl; and receives patent royalties from Labcorp and Bayer. J.A.D. has received
897 research support from Rain Therapeutics, Inc. and is a consultant for Rain
898 Therapeutics, Inc. and Takeda, Inc.

899

900 **Funding**
901 This work was supported in part by the US Public Health Service grants R35CA232128
902 and P01CA203655 and by the Bridge Project, a partnership between the Koch Institute
903 for Integrative Cancer Research at MIT and the Dana-Farber/Harvard Cancer Center to

904 J.A.D.; a Cancer Grand Challenges OPTIMISTICC team award (C10674/A27140) and
905 by National Cancer Institute grant R35CA197568 to M.M.; R01 AI060584 and R21
906 AI147155 to M.J.I; CD & SV were supported by R35GM134944; GJS is supported by
907 the NIH Intramural Research Program.

908

909 **Authors' Contributions**

910 Conceptualization - J.N., M.M., J.A.D.

911 Data curation - J.N.

912 Formal analysis - J.N.

913 Funding acquisition - M.M, J.A.D., M.J.I., S.V., G.J.S.

914 Investigation - J.N., W.Z., T.C.F., C.D.

915 Methodology - J.N., M.M., J.A.D.

916 Project administration - J.N.

917 Resources - J.N., M.M., J.A.D., T.C.F., W.Z., M.J.I, S.V., C.D.

918 Software - J.N.

919 Supervision - M.M., J.A.D.

920 Validation - J.N.

921 Visualization - J.N.

922 Writing, Original draft - J.N., M.M., J.A.D.

923 Writing, review & editing - J.N., W.Z., T.C.F., C.D., S.V., G.J.S., M.J.I., M.M., J.A.D.

924

925 **Acknowledgements**

926 We thank Katie Vicari (www.KatieRisVicari.com) for her work illustrating Figure 1A, 2, 3,
927 and S12B. Figure 1F was made in BioRender. We thank Mary O'Reilly with the Broad
928 Research Communication Lab for helpful discussions on figure design. We thank
929 Robert Garcea and Kimberly Erickson for kindly providing stocks of MPyV. Portions of
930 this research were conducted using the O2 High Performance Computing Cluster,
931 supported by the Research Computing Group at Harvard Medical School. Portions of
932 this work utilized the computational resources of the NIH HPC Biowulf cluster
933 (<http://hpc.nih.gov>).

934

935 **Figure legends**

936 **Figure 1** - RNA sequencing expands known SV40 and BKPyV transcript diversity.

937 **A.** Overview of experimental procedures. Cells were infected with a polyomavirus,
938 and RNAs extracted. RNA was sequenced using long-read (Nanopore dRNAseq
939 and PacBio SMRTseq) and short-read (Illumina short-RNAseq (total) and short-
940 RNAseq (polyA)). Transcripts were analyzed, and the impact of observed splice
941 events on viral open reading frames was assessed.

942 **B.** Mechanism of transcript clustering in this study. Transcripts were aligned to the
943 viral genome and grouped into transcript classes based on the presence of

944 shared introns. Thus, within a transcript class there may be variation in the exact
945 transcript start and end positions. This clustering strategy was used for both long-
946 and short-RNAseq data.

947 **C.** Viral RNA sequence coverage for SV40 and BKPyV as determined from
948 dRNAseq, SMRTseq, and short-RNAseq (total) data. The Y axis indicates the
949 scaled coverage, with X axis indicating the position on the viral genome.
950 Coverage for late transcripts (mapping to the + strand) is above the x axis, while
951 coverage for early transcripts (mapping to the - strand) is below the x axis.
952 Coverage is scaled separately for each strand such that the maximum observed
953 coverage for each strand is 1. Arrows at the top of the plot indicate the positions
954 of viral genes.

955 **D-E.** UpSet plot indicating the overlap between existing transcript annotations,
956 dRNAseq data, and SMRTseq data for SV40 (**D**) and BKPyV Dunlop (**E**). Bars
957 indicating overlap with existing transcript annotations are black, while those
958 indicating no overlap with existing annotations are blue. These blue bars indicate the
959 number of novel, unannotated transcripts identified.

960 **F.** Overview of polysome profiling of SV40-infected cells. BSC40 cells were
961 infected with SV40. Cells were lysed, and a portion of the lysate was subjected to
962 dRNAseq (representative of the RNA content of the whole cell). The remaining
963 lysates was centrifuged through a sucrose gradient, after which fractions
964 containing RNA associated with two or more ribosomes were pooled and
965 subjected to dRNAseq.

966 **G.** Relative abundance of SV40 early and late transcripts in the whole-cell and
967 polysome fractions of SV40-infected cells. Y-axis indicates the percentage of
968 early or late transcripts and is log scale. X axis indicates each transcript, with
969 black dots indicating each transcript's whole-cell relative abundance and red dots
970 indicating each transcript's polysome relative abundance.

971

972 **Figure 2** - Annotated and novel SV40 transcripts.

973 **A.** Transcripts are shown relative to the viral genome. Each line is a viral transcript,
974 with red lines indicating exons and dashed blue lines indicating introns. Spokes
975 indicate the positions of common splice donors and splice acceptors. Transcripts
976 that were annotated prior to this study are on a yellow background, and novel
977 transcripts are on a white background. Wraparound transcription that results in
978 multiple copies of a region is annotated with double lines, and the number of
979 copies is indicated in parentheses. The line labeled "pA" indicates the
980 approximate position of the polyA signal sequence.

981 **Figure 3** - Annotated and novel BKPyV transcripts.

982 **A.** Transcripts are shown relative to the viral genome. Each line is a viral transcript,
983 with red lines indicating exons and dashed blue lines indicating introns. Spokes
984 indicate the positions of common splice donors and splice acceptors. Transcripts
985 that were annotated prior to this study are on a yellow background, and novel
986 transcripts are on a white background. Wraparound transcription that results in
987 multiple copies of a region is annotated with double lines, and the number of

988 copies is indicated in parentheses. The line labeled “pA” indicates the
989 approximate position of the polyA signal sequence.

990

991 **Figure 4** - Pervasive wraparound transcription across PyV

992 **A-C.** Watch plots indicating the top 4 highest abundance late wraparound
993 transcript classes in dRNAseq data from SV40 (A), BKPyV Dunlop (B), and
994 MPyV (C). The outer ring of each watch plot indicates the position of the viral
995 ORFs. The inner arms are histograms detailing the distribution of transcript starts
996 (in blue) and ends (in red) for transcripts within each transcript class. The red
997 segments indicate exons. Transcripts start in the innermost ring - a second or
998 third ring indicates that the pre-mRNA that generated the transcript must have
999 circled the viral genome multiple times. The 3' end of the transcript and the
1000 direction in which these plots are oriented is indicated by the red arrow at the end
1001 of the last exon segment. The red exon segments start at the most common
1002 transcript start site within the transcript class, and end at the most common
1003 transcript end site within the class. The watch plot key shows an example of the
1004 path of the pre-mRNA for SV40 transcript class L6_I.

1005 **D.** Bar plots indicating the percentage of late transcripts that span a given number of
1006 genome lengths in SV40, BKPyV Dunlop, and MPyV dRNAseq data.

1007 **E.** The leader-leader junction, that connects the pre-mRNA from one genome to the
1008 subsequent wraparound, was identified in Illumina short-RNAseq (total) data.
1009 The intron in question is plotted as a black line in this plot, with the x axis

1010 indicating the genomic position of the intron. The top late wraparound transcript
1011 for each virus was plotted. The gene map indicates the approximate gene
1012 position and is accurate for SV40 - the exact position of the viral genes varies
1013 between viruses. Percentages indicate the percentage of late junction-spanning
1014 transcripts that support the plotted wraparound leader-leader junction.

1015 **F.** Schematic illustrating how leader-leader wraparound transcription can be
1016 detected from short read short-RNAseq (total). Leader-leader splicing can be
1017 seen as a repetitive exon in watch plots from long-read RNAseq data. Ultimately,
1018 there was an original processed mRNA in the cell that contained two tandem
1019 leader sequences. When this transcript of origin is sequenced via short read
1020 sequencing, reads will be generated across its length. A minority of these reads
1021 will span the leader-leader junction, and mapping against the viral reference
1022 genome can be used to uncover leader-leader splicing.

1023 **Figure 5** - Detection of novel, conserved splicing events that expand PyV coding
1024 capacity.

1025 **A-D.** Schematics illustrating identified ORFs. Each row is a reading frame (except for
1026 ST and the LT 1st exon, which are in the same frame), and unannotated amino acids are
1027 represented by grey boxes. The measured intron is indicated by the red arrow. Colored
1028 ORFs are annotated, while grey ORFs are unannotated. Percentages on the right side
1029 of the figure are the percentage of spliced viral transcripts on the same strand as
1030 determined from short-read short-RNAseq (total) data. Numbers after each virus name
1031 indicate the transcript class within each short-RNAseq (total) dataset. The measured
1032 intron is indicated by the red arrow.

1033 A) ST2: This ORF is generating from a splicing event that uses the LT first exon
1034 donor and an acceptor within the ST ORF. In HPyV7 and BKPyV Dunlop, the splice
1035 lands in frame and results in an internal deletion within ST. In MPyV and MCPyV the
1036 splice lands out of frame, resulting in an ORF that contains the N-terminal region of
1037 ST and novel amino acids at the C terminus.

1038 B) MT: MPyV encodes a MT following splicing connecting the end of the ST ORF
1039 with an ORF in an alternate frame of the LT second exon. In BKPyV, a similar splice
1040 occurs connecting ST with an MT-like ORF in an alternative frame of the LT second
1041 exon.

1042 C) VP1X: JCPyV encodes two VP1X ORFs generated by splicing within VP1 and
1043 landing in an alternative frame of VP1, or earlier in the late region due to wraparound
1044 transcription. While predominant in JCPyV, VP1X is likewise present in many other
1045 PyV.

1046 D) superT: The superT-specific splice utilizes the splice donor canonically
1047 associated with truncated T antigens such as 17kT in SV40 and truncT in BKPyV.
1048 Due to wraparound transcription, a LT second exon acceptor is available to the 3' of
1049 this donor and acts as the acceptor. For the superT ORF to form, an initial LT splice
1050 is required. Ultimately, superT contains a duplication in part of the LT second exon
1051 that includes the RB-binding LxCxE motif.

1052 E. Schematics detailing BKPyV Dik isolates used for querying the existence of superT.
1053 BKPyV WT is wild type virus. M1 contains a LT intron that has been replaced with an
1054 intron from the plasmid pCI. Both WT and M1 are expected to generate LT and superT

1055 of expected sizes. M2 has a completely removed LT intron, and the pCI intron is located
1056 directly 5' of the LT ORF. M2 is expected to encode LT of expected size, but a larger
1057 superT variant due to incorporation of a second copy of the LT first exon.

1058 **F.** Western blot of cells infected with BKPyV Dik WT, M1, or M2 and probed with an
1059 antibody reactive against LT. The lower molecular weight band is LT, and the higher
1060 molecular weight bands are consistent with superT.

1061

1062 **Figure 6** - Detection superT-encoding transcripts in PyV-associated cancers

1063 **A.** Schematic detailing the generation of superT during lytic infection as compared
1064 to from integrated virus in cancer. During viral infection, the RNA polymerase can
1065 circle the viral genome multiple times, resulting in a pre-mRNA that can be
1066 spliced to generate superT. In the case of host integration, a polyomavirus can
1067 be integrated in tandem copies such that a pre-mRNA is generated with more
1068 than one copy of the viral early region. This pre-mRNA can be similarly spliced to
1069 generate a superT transcript.

1070 **B.** Heatmap indicating the abundance of the superT, ST, and LT introns from
1071 RNAseq data from two replicates of a BKPyV-positive bladder cancer and six
1072 MCPyV-associated MCCs. Percentages indicate the percentage of spliced early
1073 viral reads for each sample. The splice measured in each row is indicated by the
1074 red arrow in the schematics on the right side of the figure.

1075

1076 **Figure S1** - Sequencing statistics

1077 **A.** The number of reads for all datasets studied here. For long-read dRNAseq and
1078 SMRTseq, this number includes spliced and unspliced reads. Because short
1079 reads are only useful for transcript characterization when they span a splice
1080 junction, the counts for short-reads represent the number of splice-junction-
1081 spanning reads.

1082 **B.** The cumulative percentage of transcripts in each number of transcript classes, by
1083 strand. The X-axis indicated the total number of transcript classes. The Y axis
1084 indicates the cumulative percentage of transcripts within those transcript classes.
1085 These plots indicate that most transcripts in most samples are contained within
1086 the first few transcript classes.

1087 **C-E.** The alignment length distribution of early, late, spliced, and unspliced
1088 transcripts for dRNAseq and SMRTseq data from SV40 (**C**), BKPyV Dunlop (**D**), and
1089 MPyV (**E**). The X axis indicates the length of a read's alignment, while the Y axis
1090 indicates the density/percentage of transcripts with a given alignment length. This
1091 plot shows that dRNAseq and SMRTseq data sample from RNA populations of
1092 different length.

1093

1094 **Figure S2** - Transcript start sites and polyA tail lengths.

1095 **A, B.** The distribution of transcript start sites for late (**A**) and early (**B**) transcripts for
1096 SV40 (left column), BKPyV Dunlop (middle column), and MPyV (right column). The
1097 arrows indicate the viral ORF positions.

1098 **C.** The distribution of polyA tail lengths for the 30-adenine ENO2 control (black),
1099 host (red), and viral (yellow) transcripts for SV40, BKPyV Dunlop, and MPyV.
1100 The X axis indicates the length of the polyA tail, while the Y axis indicates the
1101 density/percentage of transcripts with each length.
1102 **D.** Ribosome occupancy of host transcripts in SV40-infected cells. Each grey dot is
1103 a host transcript. The red, blue, and black dots are specifically noted host
1104 transcripts. Ribosome occupancy is on the Y axis, while the X axis does not hold
1105 value. Lines on the violin plot indicate 1st, 2nd, and 3rd quartiles.

1106

1107 **Figure S3** - SV40 transcriptome atlas, watch plots

1108 **A-C.** Watch plots indicating all identified transcripts in SV40. **(A)** and **(B)** show
1109 transcripts that were identified in both dRNAseq and SMRTseq data, while **(C)**
1110 shows transcripts identified in SMRTseq only.

1111 **E.** Barplots that show the abundance of each transcript type in the dRNAseq and
1112 SMRTseq data. Here, there are two dRNAseq bars (one per replicate). The Y
1113 axis indicates the percentage of transcripts of the same strand. As discussed in
1114 the methods, alignment of superT and superT* was challenging, so the actual
1115 abundance of these transcripts is higher than reported here.

1116

1117 **Figure S4** - BKPyV Dunlop transcriptome atlas, watch plots

1118 **A-C.** Watch plots indicating all identified transcripts in BKPyV Dunlop. **(A)** and
1119 **(B)** show transcripts that were identified in both dRNASeq and SMRTseq data,
1120 while **(C)** shows transcripts identified in dRNASeq only.

1121 **F.** Barplots that show the abundance of each transcript type in the dRNASeq and
1122 SMRTseq data. The Y axis indicates the percentage of transcripts of the same
1123 strand. As discussed in the methods, alignment of superT and superT* was
1124 challenging, so the actual abundance of these transcripts is higher than reported
1125 here.

1126

1127 **Figure S5** - SV40 transcriptome atlas, late transcript read pileups

1128 **A, B.** Read pileups showing the late transcripts identified in SV40 dRNASeq (A)
1129 and SMRTseq (B). The arrows at the top of the plot indicate the viral ORF
1130 positions. Below the X axis, each row is an individual transcript, with exons
1131 indicated in red and splice junctions/introns indicated in pink. Above the X axis
1132 are histograms indicating the transcript start (blue) and transcript end (red) sites.
1133 (U: unspliced).

1134

1135 **Figure S6** - SV40 transcriptome atlas, early transcript read pileups

1136 **A, B.** Read pileups showing the early transcripts identified in SV40 dRNASeq (A)
1137 and SMRTseq (B). The arrows at the top of the plot indicate the viral ORF
1138 positions. Below the X axis, each row is an individual transcript, with exons

1139 indicated in red and splice junctions/introns indicated in pink. Above the X axis
1140 are histograms indicating the transcript start (blue) and transcript end (red) sites.
1141 (U: unspliced).

1142

1143 **Figure S7** - BKPyV Dunlop transcriptome atlas, late transcript read pileups

1144 **A, B.** Read pileups showing the late transcripts identified in BKPyV Dunlop
1145 dRNAseq (A) and SMRTseq (B). The arrows at the top of the plot indicate the
1146 viral ORF positions. Below the X axis, each row is an individual transcript, with
1147 exons indicated in red and splice junctions/introns indicated in pink. Above the X
1148 axis are histograms indicating the transcript start (blue) and transcript end (red)
1149 sites. (U: unspliced).

1150

1151 **Figure S8** - BKPyV Dunlop transcriptome atlas, early transcript read pileups

1152 **A, B.** Read pileups showing the early transcripts identified in BKPyV Dunlop
1153 dRNAseq (A) and SMRTseq (B). The arrows at the top of the plot indicate the
1154 viral ORF positions. Below the X axis, each row is an individual transcript, with
1155 exons indicated in red and splice junctions/introns indicated in pink. Above the X
1156 axis are histograms indicating the transcript start (blue) and transcript end (red)
1157 sites. (U: unspliced).

1158

1159 **Figure S9** - Intron plots for all datasets studied

1160 A. Intron plots generated from short-read RNAseq. The arrows at the top and
1161 bottom of each panel indicate the position of viral ORFs. The lines indicate
1162 specific introns identified in the RNAseq data, with the 5' end on the top and the
1163 3' end on the bottom. The blue color indicates late transcripts, with red indicating
1164 early transcripts. The size of the circles above and below the viral ORF maps
1165 indicate the percentage of junction-spanning reads with a 5' end (on top) or 3'
1166 end (on bottom) at that position. Junctions are plotted if they are at least 1% of
1167 early or late transcripts, except for the SV40 pA superT junction (transcript class
1168 3) which is just below threshold but is of interest.

1169 B. Another representation of intron plots for each virus. The top arrows indicate the
1170 position of viral ORFs. The X axis indicates the genomic position for each splice.
1171 The Y axis indicates a single transcript class, with that class' intron plotted as a
1172 line. The percentage of early or late transcripts is indicated with the numeric
1173 percentage. Junctions are plotted if they are at least 1% of early or late
1174 transcripts, except for the SV40 pA superT junction (transcript class 3) which is
1175 just below threshold but is of interest.

1176

1177 **Figure S10** - Alternative polyadenylation of early transcripts in SV40, BKPyV, and
1178 MPyV.

1179 **A-C.** Watch plots indicating the LT and ST transcripts for SV40 (**A**), BKPyV
1180 Dunlop (**B**), and MPyV (**C**). The focus of these plots is the distribution of
1181 transcript end positions, which are the inner red arms. The region of APA of
1182 highlighted in blue, with the canonical transcript end sites highlighted in red.

1183 **D.** A cumulative incidence plot of transcript termination in SV40 (blue), BKPyV
1184 Dunlop (red), and MPyV (green). The X axis indicates the distance to the
1185 canonical polyA site, while the Y axis indicates the percentage of transcripts that
1186 have terminated by that position.

1187 **E-G.** Density plots showing the distribution of polyA tail lengths for LT and ST
1188 transcripts that end at the canonical site (solid) or undergo APA (dashed) for
1189 SV40 (**E**), BKPyV Dunlop (**F**), and MPyV (**G**). The x axis indicates the length of
1190 the polyA tail, while the Y axis indicates the density/proportion of transcripts with
1191 the given length.

1192

1193 **Figure S11** - short-RNAseq (polyA) analysis of BKPyV Dik WT, M1, and M2

1194 **A-C.** Intron plots generated from short-read (polyA) RNAseq of cells infected with
1195 BKPyV WT, or the M1 or M2 mutants. The arrows at the top and bottom of each panel
1196 indicate the position of viral ORFs relative to the standard BKPyV genome - note that
1197 the genomes of mutants M1 and M2 are altered as indicated in Figure 5E. The lines
1198 indicate specific introns identified in the RNAseq data, with the 5' end on the top and the
1199 3' end on the bottom. The size of the circles above and below the viral ORF maps
1200 indicate the percentage of junction-spanning reads with a 5' end (on top) or 3' end (on
1201 bottom) at that position. Only early junctions that are at least 1% of early early
1202 transcripts are plotted. The superT junction is colored in gold. (**A**) Intron plot for BKPyV
1203 Dik WT. (**B**) Intron plot for BKPyV Dik M1. (**C**) Intron plot for BKPyV Dik M2.

1204

1205 **Figure S12 - superT in MCPyV-associated MCC**

- 1206 A. Sanger sequencing of an RT-PCR product from MCC J45_440, showing the
1207 superT-specific junction.
- 1208 B. A schematic detailing the MCC 285 MCPyV integration site, showing how it is
1209 possible that superT is generated via cis-splicing.
- 1210 C. The assembled viral block in MCC tumor J45_440. This integration site is based
1211 on de-novo assembly using short whole genome sequencing reads. Despite only
1212 assembling one viral block, we found that 1) there are likely 2 copies of the viral
1213 genome, and 2) the 5' viral integration site appears to fall on chromosome 7
1214 "after" the 3' viral integration site, observations consistent with the existence of
1215 two copies of the viral genome in tandem separated by a small segment of host
1216 DNA at this integration site.
- 1217 D. The assembled viral blocks in MCC tumor J17_296. The longest block contains
1218 two copies of the early region.
- 1219 E. Lollipop plots showing identified SNPs in the MCPyV genomes of J45_440,
1220 J17_296, and J11_285. The gene-map below the figure indicates the position of
1221 viral ORFs. Each lollipop is colored according to the nucleotide substitution
1222 identified.
- 1223
- 1224

- 1225 Abend, J.R., Joseph, A.E., Das, D., Campbell-Cecen, D.B., and Imperiale, M.J. (2009).
- 1226 A truncated T antigen expressed from an alternatively spliced BK virus early mRNA.
- 1227 The Journal of general virology 90, 1238.
- 1228 Abere, B., Zhou, H., Li, J., Cao, S., Toptan, T., Grundhoff, A., Fischer, N., Moore, P.S.,
- 1229 and Chang, Y. (2020). Merkel Cell Polyomavirus Encodes Circular RNAs (circRNAs)
- 1230 Enabling a Dynamic circRNA/microRNA/mRNA Regulatory Network. *Mbio* 11, e03059-
- 1231 03020.
- 1232 Adami, G., Marlor, C., Barrett, N., and Carmichael, G.G. (1989). Leader-to-leader
- 1233 splicing is required for efficient production and accumulation of polyomavirus late
- 1234 mRNAs. *Journal of virology* 63, 85-93.
- 1235 Assetta, B., De Cecco, M., O'Hara, B., and Atwood, W.J. (2016). JC polyomavirus
- 1236 infection of primary human renal epithelial cells is controlled by a type I IFN-induced
- 1237 response. *MBio* 7, e00903-00916.
- 1238 Balázs, Z., Tombácz, D., Szűcs, A., Snyder, M., and Boldogkői, Z. (2017). Long-read
- 1239 sequencing of the human cytomegalovirus transcriptome with the Pacific Biosciences
- 1240 RSII platform. *Scientific data* 4, 1-7.
- 1241 Carter, J.J., Daugherty, M.D., Qi, X., Bheda-Malge, A., Wipf, G.C., Robinson, K.,
- 1242 Roman, A., Malik, H.S., and Galloway, D.A. (2013). Identification of an overprinting
- 1243 gene in Merkel cell polyomavirus provides evolutionary insight into the birth of viral
- 1244 genes. *Proceedings of the National Academy of Sciences* 110, 12744-12749.

- 1245 Depledge, D.P., Srinivas, K.P., Sadaoka, T., Bready, D., Mori, Y., Placantonakis, D.G.,
- 1246 Mohr, I., and Wilson, A.C. (2019). Direct RNA sequencing on nanopore arrays redefines
- 1247 the transcriptional complexity of a viral pathogen. *Nature communications* 10, 1-13.
- 1248 Dobin, A., Davis, C.A., Schlesinger, F., Drenkow, J., Zaleski, C., Jha, S., Batut, P.,
- 1249 Chaisson, M., and Gingeras, T.R. (2013). STAR: ultrafast universal RNA-seq aligner.
- 1250 *Bioinformatics* 29, 15-21.
- 1251 Eul, J., and Patzel, V. (2013). Homologous SV40 RNA trans-splicing: a new mechanism
- 1252 for diversification of viral sequences and phenotypes. *RNA biology* 10, 1689-1699.
- 1253 Freund, R., Sotnikov, A., Bronson, R.T., and Benjamin, T.L. (1992). Polyoma virus
- 1254 middle T is essential for virus replication and persistence as well as for tumor induction
- 1255 in mice. *Virology* 191, 716-723.
- 1256 Garalde, D.R., Snell, E.A., Jachimowicz, D., Sipos, B., Lloyd, J.H., Bruce, M., Pantic, N.,
- 1257 Admassu, T., James, P., and Warland, A. (2018). Highly parallel direct RNA sequencing
- 1258 on an array of nanopores. *Nature methods* 15, 201-206.
- 1259 Garren, S.B., Kondaveeti, Y., Duff, M.O., and Carmichael, G.G. (2015). Global analysis
- 1260 of mouse polyomavirus infection reveals dynamic regulation of viral and host gene
- 1261 expression and promiscuous viral RNA editing. *PLoS pathogens* 11, e1005166.
- 1262 Ghosh, P., Reddy, V., Swinscoe, J., Lebowitz, P., and Weissman, S. (1978).
- 1263 Heterogeneity and 5'-terminal structures of the late RNAs of simian virus 40. *Journal of*
- 1264 *molecular biology* 126, 813-846.

- 1265 Good, P.J., Welch, R.C., Ryu, W.-S., and Mertz, J.E. (1988). The late spliced 19S and
1266 16S RNAs of simian virus 40 can be synthesized from a common pool of transcripts.
1267 Journal of virology 62, 563-571.
- 1268 Gottlieb, K.A., and Villarreal, L.P. (2001). Natural biology of polyomavirus middle T
1269 antigen. Microbiology and molecular biology reviews 65, 288-318.
- 1270 Jiang, M., Abend, J.R., Johnson, S.F., and Imperiale, M.J. (2009a). The role of
1271 polyomaviruses in human disease. Virology 384, 266-273.
- 1272 Jiang, M., Abend, J.R., Tsai, B., and Imperiale, M.J. (2009b). Early events during BK
1273 virus entry and disassembly. Journal of virology 83, 1350-1358.
- 1274 Johnson, M., Zaretskaya, I., Raytselis, Y., Merezhuk, Y., McGinnis, S., and Madden,
1275 T.L. (2008). NCBI BLAST: a better web interface. Nucleic acids research 36, W5-W9.
- 1276 Kamen, R., Favaloro, J., and Parker, J. (1980a). Topography of the three late mRNA's
1277 of polyoma virus which encode the virion proteins. Journal of virology 33, 637-651.
- 1278 Kamen, R., Favaloro, J., Parker, J., Treisman, R., Lania, L., Fried, M., and Mellor, A.
1279 (1980b). Comparison of polyoma virus transcription in productively infected mouse cells
1280 and transformed rodent cell lines. Paper presented at: Cold Spring Harbor symposia on
1281 quantitative biology (Cold Spring Harbor Laboratory Press).
- 1282 Keller, M.W., Rambo-Martin, B.L., Wilson, M.M., Ridenour, C.A., Shepard, S.S., Stark,
1283 T.J., Neuhaus, E.B., Dugan, V.G., Wentworth, D.E., and Barnes, J.R. (2018). Direct
1284 RNA sequencing of the coding complete influenza A virus genome. Scientific reports 8,
1285 1-8.

- 1286 Kim, D., Lee, J.-Y., Yang, J.-S., Kim, J.W., Kim, V.N., and Chang, H. (2020). The
1287 architecture of SARS-CoV-2 transcriptome. *Cell* *181*, 914-921. e910.
- 1288 Kress, M., May, E., Cassingena, R., and May, P. (1979). Simian virus 40-transformed
1289 cells express new species of proteins precipitable by anti-simian virus 40 tumor serum.
1290 *Journal of virology* *31*, 472-483.
- 1291 Krueger, F. (2016). Babraham Bioinformatics-Trim Galore.
- 1292 Lee, S., Micalizzi, D., Truesdell, S.S., Bukhari, S.I., Boukhali, M., Lombardi-Story, J.,
1293 Kato, Y., Choo, M.-K., Dey-Guha, I., and Ji, F. (2020). A post-transcriptional program of
1294 chemoresistance by AU-rich elements and TTP in quiescent leukemic cells. *Genome*
1295 *biology* *21*, 1-23.
- 1296 Legon, S., Flavell, A.J., Cowie, A., and Kamen, R. (1979). Amplification in the leader
1297 sequence of late polyoma virus mRNAs. *Cell* *16*, 373-388.
- 1298 Li, H. (2018). Minimap2: pairwise alignment for nucleotide sequences. *Bioinformatics*
1299 *34*, 3094-3100.
- 1300 Loman, N.J., Quick, J., and Simpson, J.T. (2015). A complete bacterial genome
1301 assembled de novo using only nanopore sequencing data. *Nature methods* *12*, 733-
1302 735.
- 1303 Luo, Y., and Carmichael, G.G. (1991). Splice site skipping in polyomavirus late pre-
1304 mRNA processing. *Journal of virology* *65*, 6637-6644.
- 1305 Nguyen, K.D., Lee, E.E., Yue, Y., Stork, J., Pock, L., North, J.P., Vandergriff, T.,
1306 Cockerell, C., Hosler, G.A., and Pastrana, D.V. (2017). Human polyomavirus 6 and 7

- 1307 are associated with pruritic and dyskeratotic dermatoses. *Journal of the American*
1308 *Academy of Dermatology* **76**, 932-940. e933.
- 1309 Nomburg, J., Meyerson, M., and DeCaprio, J.A. (2020). Pervasive generation of non-
1310 canonical subgenomic RNAs by SARS-CoV-2. *Genome medicine* **12**, 1-14.
- 1311 Norbury, C.J., and Fried, M. (1987). Polyomavirus early region alternative poly (A) site:
1312 3'-end heterogeneity and altered splicing pattern. *Journal of virology* **61**, 3754-3758.
- 1313 Price, A.M., Hayer, K.E., McIntyre, A.B., Gokhale, N.S., Abebe, J.S., Della Fera, A.N.,
1314 Mason, C.E., Horner, S.M., Wilson, A.C., and Depledge, D.P. (2020). Direct RNA
1315 sequencing reveals m 6 A modifications on adenovirus RNA are necessary for efficient
1316 splicing. *Nature communications* **11**, 1-17.
- 1317 Quinlan, A.R., and Hall, I.M. (2010). BEDTools: a flexible suite of utilities for comparing
1318 genomic features. *Bioinformatics* **26**, 841-842.
- 1319 Reddy, V.B., Ghosh, P.K., Lebowitz, P., and Sherman M, W. (1978). Gaps and
1320 duplicated sequences in the leaders of SV40 16S RNA. *Nucleic acids research* **5**, 4195-
1321 4214.
- 1322 Riley, M.I., Yoo, W., Mda, N.Y., and Folk, W.R. (1997). Tiny T antigen: an autonomous
1323 polyomavirus T antigen amino-terminal domain. *Journal of virology* **71**, 6068-6074.
- 1324 Rosenstein, R.K., Pastrana, D.V., Starrett, G.J., Sapiro, M.R., Hill, N.T., Jo, J.-H., Lee,
1325 C.-C.R., Iadarola, M.J., Buck, C.B., and Kong, H.H. (2021). Host-Pathogen Interactions
1326 in Human Polyomavirus 7-Associated Pruritic Skin Eruption. *The Journal of*
1327 *investigative dermatology* **141**, 1344-1348. e1348.

- 1328 Saribas, A.S., DeVoto, J., Golla, A., Wollebo, H.S., White, M.K., and Safak, M. (2018).
1329 Discovery and characterization of novel trans-spliced products of human polyoma JC
1330 virus late transcripts from PML patients. *Journal of cellular physiology* 233, 4137-4155.
1331 Schmidlin, K., Krabberger, S., Cook, C., DeNardo, D.F., Fontenele, R.S., Van Doorslaer,
1332 K., Martin, D.P., Buck, C.B., and Varsani, A. (2021). A novel lineage of polyomaviruses
1333 identified in bark scorpions. *bioRxiv*.
1334 Seif, I., Khoury, G., and Dhar, R. (1979). The genome of human papovavirus BKV. *Cell*
1335 18, 963-977.
1336 Shuda, M., Feng, H., Kwun, H.J., Rosen, S.T., Gjoerup, O., Moore, P.S., and Chang, Y.
1337 (2008). T antigen mutations are a human tumor-specific signature for Merkel cell
1338 polyomavirus. *Proceedings of the National Academy of Sciences* 105, 16272-16277.
1339 Smith, A.E., Smith, R., and Paucha, E. (1979). Characterization of different tumor
1340 antigens present in cells transformed by simian virus 40. *Cell* 18, 335-346.
1341 Starrett, G.J., Thakuria, M., Chen, T., Marcelus, C., Cheng, J., Nomburg, J., Thorner,
1342 A.R., Slevin, M.K., Powers, W., and Burns, R.T. (2020). Clinical and molecular
1343 characterization of virus-positive and virus-negative Merkel cell carcinoma. *Genome*
1344 *medicine* 12, 1-22.
1345 Starrett, G.J., Yu, K., Golubeva, Y., Lenz, P., Piaskowski, M.L., Peterson, D., Dean, M.,
1346 Israni, A., Hernandez, B.Y., Tucker, T.C., *et al.* (2021). Common Mechanisms of Virus-
1347 Mediated Oncogenesis in Bladder Cancers Arising In Solid Organ Transplant
1348 Recipients. *medRxiv*, 2021.2011.2011.21266080.

- 1349 Theiss, J.M., Günther, T., Alawi, M., Neumann, F., Tessmer, U., Fischer, N., and
- 1350 Grundhoff, A. (2015). A comprehensive analysis of replicating Merkel cell polyomavirus
- 1351 genomes delineates the viral transcription program and suggests a role for mcv-miR-M1
- 1352 in episomal persistence. *PLoS pathogens* 11, e1004974.
- 1353 Treisman, R. (1980). Characterisation of polyoma late mRNA leader sequences by
- 1354 molecular cloning and DNA sequence analysis. *Nucleic acids research* 8, 4867-4888.
- 1355 Tremblay, J.D., Sachsenmeier, K.F., and Pipas, J.M. (2001). Propagation of wild-type
- 1356 and mutant SV40. In *SV40 Protocols* (Springer), pp. 1-7.
- 1357 Trowbridge, P.W., and Frisque, R.J. (1995). Identification of three new JC virus proteins
- 1358 generated by alternative splicing of the early viral mRNA. *Journal of neurovirology* 1,
- 1359 195-206.
- 1360 Yang, R., Lee, E.E., Kim, J., Choi, J.H., Kolitz, E., Chen, Y., Crewe, C., Salisbury, N.J.,
- 1361 Scherer, P.E., and Cockerell, C. (2021). Characterization of ALTO-encoding circular
- 1362 RNAs expressed by Merkel cell polyomavirus and trichodysplasia spinulosa
- 1363 polyomavirus. *PLoS pathogens* 17, e1009582.
- 1364 Zerrahn, J., Knippschild, U., Winkler, T., and Deppert, W. (1993). Independent
- 1365 expression of the transforming amino-terminal domain of SV40 large I antigen from an
- 1366 alternatively spliced third SV40 early mRNA. *The EMBO journal* 12, 4739-4746.
- 1367 Zhao, L., and Imperiale, M.J. (2019). Establishing Renal Proximal Tubule Epithelial-
- 1368 Derived Cell Lines Expressing Human Telomerase Reverse Transcriptase for Studying
- 1369 BK Polyomavirus. *Microbiology resource announcements* 8, e01129-01119.

1370 Zou, W., Vue, G.S., Assetta, B., Manza, H., Atwood, W.J., and Imperiale, M.J. (2020).

1371 Control of archetype BK polyomavirus microRNA expression. *Journal of Virology* 95,

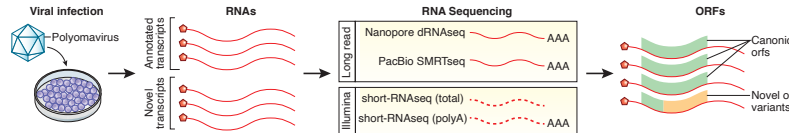
1372 e01589-01520.

1373

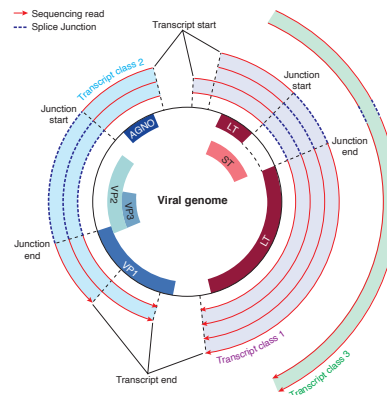
1374

Figure 1

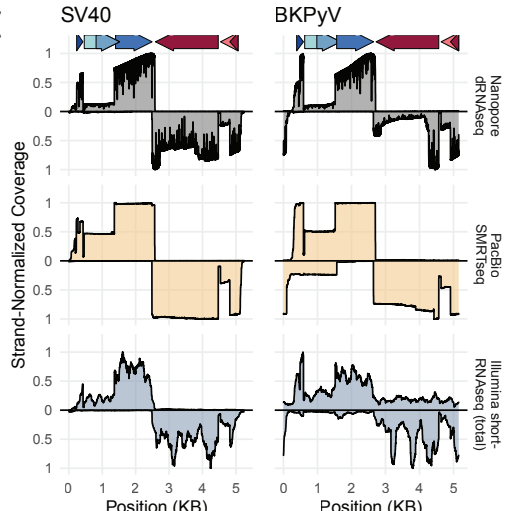
A



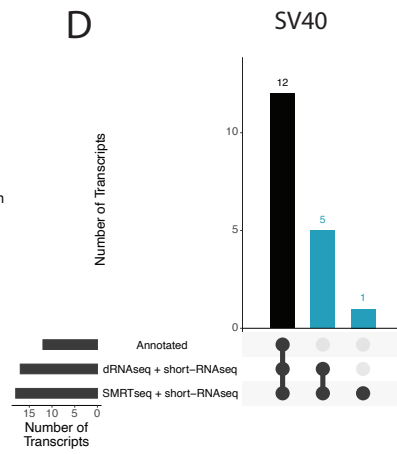
B Transcript processing strategy



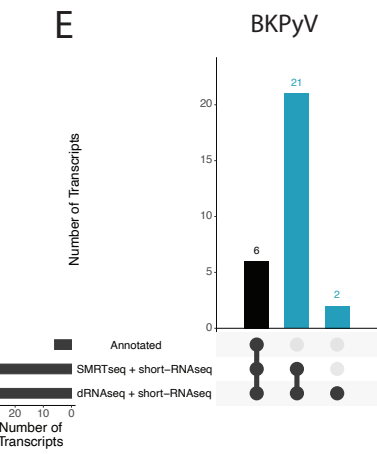
C



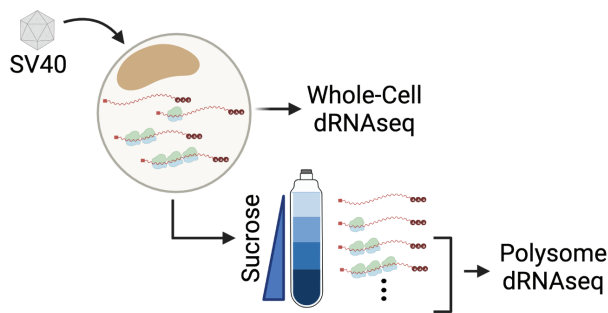
D



E



F



G

SV40 Whole-Cell vs. Polysome Transcript Abundance

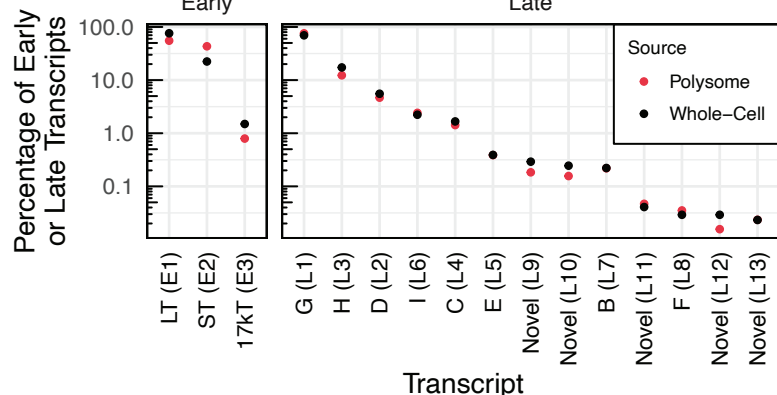


Figure 1 - RNA sequencing expands known SV40 and BKPyV transcript diversity.

A. Overview of experimental procedures. Cells were infected with a polyomavirus, and RNAs extracted. RNA was sequenced using long-read (Nanopore dRNAseq and PacBio SMRTseq) and short-read (Illumina short-RNAseq (total) and short-RNAseq (polyA)). Transcripts were analyzed, and the impact of observed splice events on viral open reading frames was assessed.

B. Mechanism of transcript clustering in this study. Transcripts were aligned to the viral genome and grouped into transcript classes based on the presence of shared introns. Thus, within a transcript class there may be variation in the exact transcript start and end positions. This clustering strategy was used for both long- and short-RNAseq data.

C. Viral RNA sequence coverage for SV40 and BKPyV as determined from dRNAseq, SMRTseq, and short-RNAseq (total) data. The Y axis indicates the scaled coverage, with X axis indicating the position on the viral genome. Coverage for late transcripts (mapping to the + strand) is above the x axis, while coverage for early transcripts (mapping to the - strand) is below the x axis. Coverage is scaled separately for each strand such that the maximum observed coverage for each strand is 1. Arrows at the top of the plot indicate the positions of viral genes.

D-E. UpSet plot indicating the overlap between existing transcript annotations, dRNAseq data, and SMRTseq data for SV40 (D) and BKPyV (E). Bars indicating overlap with existing transcript annotations are black, while those indicating no overlap with existing annotations are blue. These blue bars indicate the number of novel, unannotated transcripts identified.

F. Overview of polysome profiling of SV40-infected cells. BSC40 cells were infected with SV40. Cells were lysed, and a portion of the lysate was subjected to dRNAseq (representative of the RNA content of the whole cell). The remaining lysates was centrifuged through a sucrose gradient, after which fractions containing RNA associated with two or more ribosomes were pooled and subjected to dRNAseq.

G. Relative abundance of SV40 early and late transcripts in the whole-cell and polysome fractions of SV40-infected cells. Y-axis indicates the percentage of early or late transcripts and is log scale. X axis indicates each transcript, with black dots indicating each transcript's whole-cell relative abundance and red dots indicating each transcript's polysome relative abundance.

Figure 2

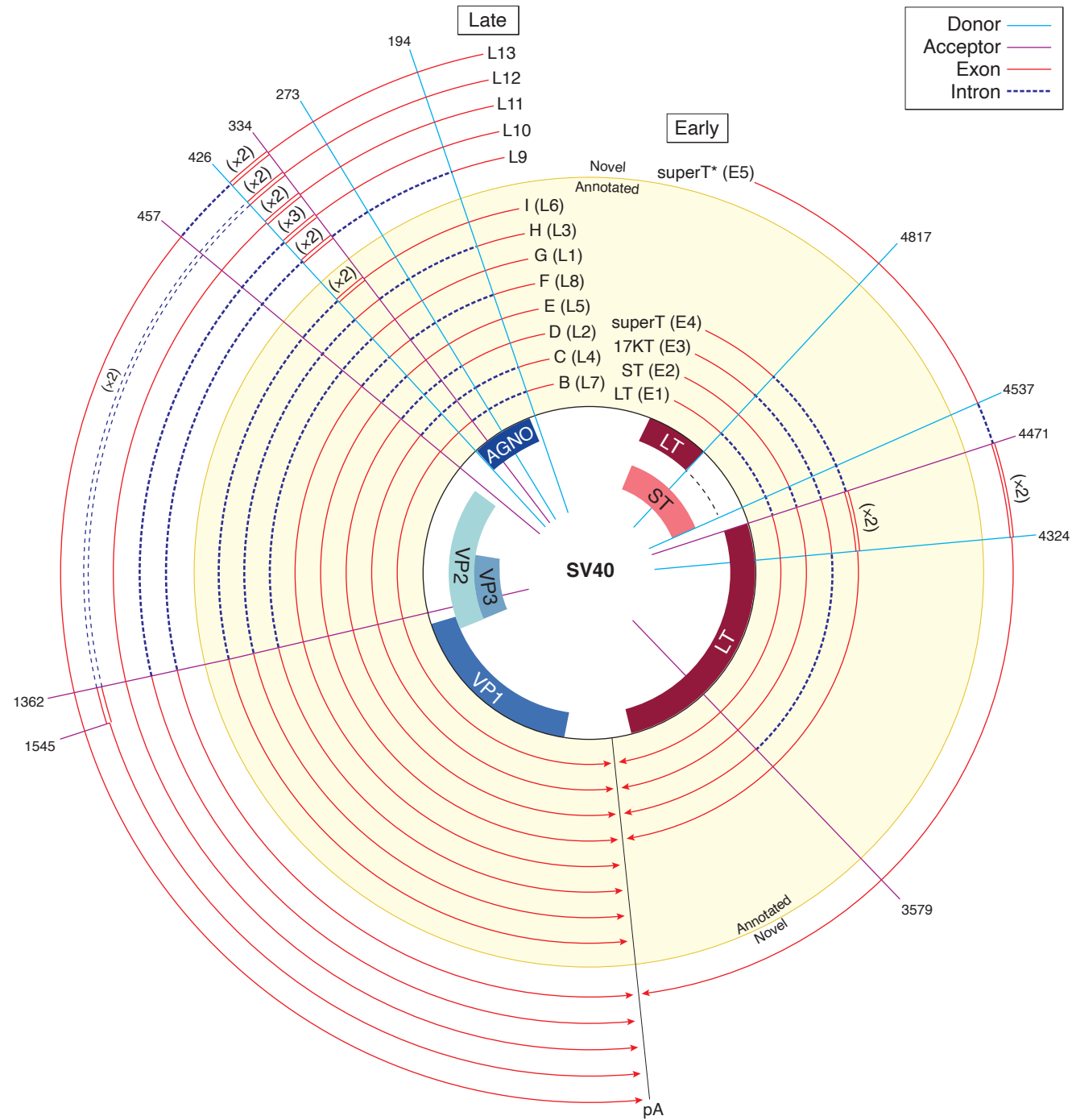


Figure 2 - Annotated and novel SV40 transcripts.

A. Transcripts are shown relative to the viral genome. Each line is a viral transcript, with red lines indicating exons and dashed blue lines indicating introns. Spokes indicate the positions of common splice donors and splice acceptors. Transcripts that were annotated prior to this study are on a yellow background, and novel transcripts are on a white background. Wraparound transcription that results in multiple copies of a region is annotated with double lines, and the number of copies is indicated in parentheses. The line labeled "pA" indicates the approximate position of the polyA signal sequence.

Figure 3

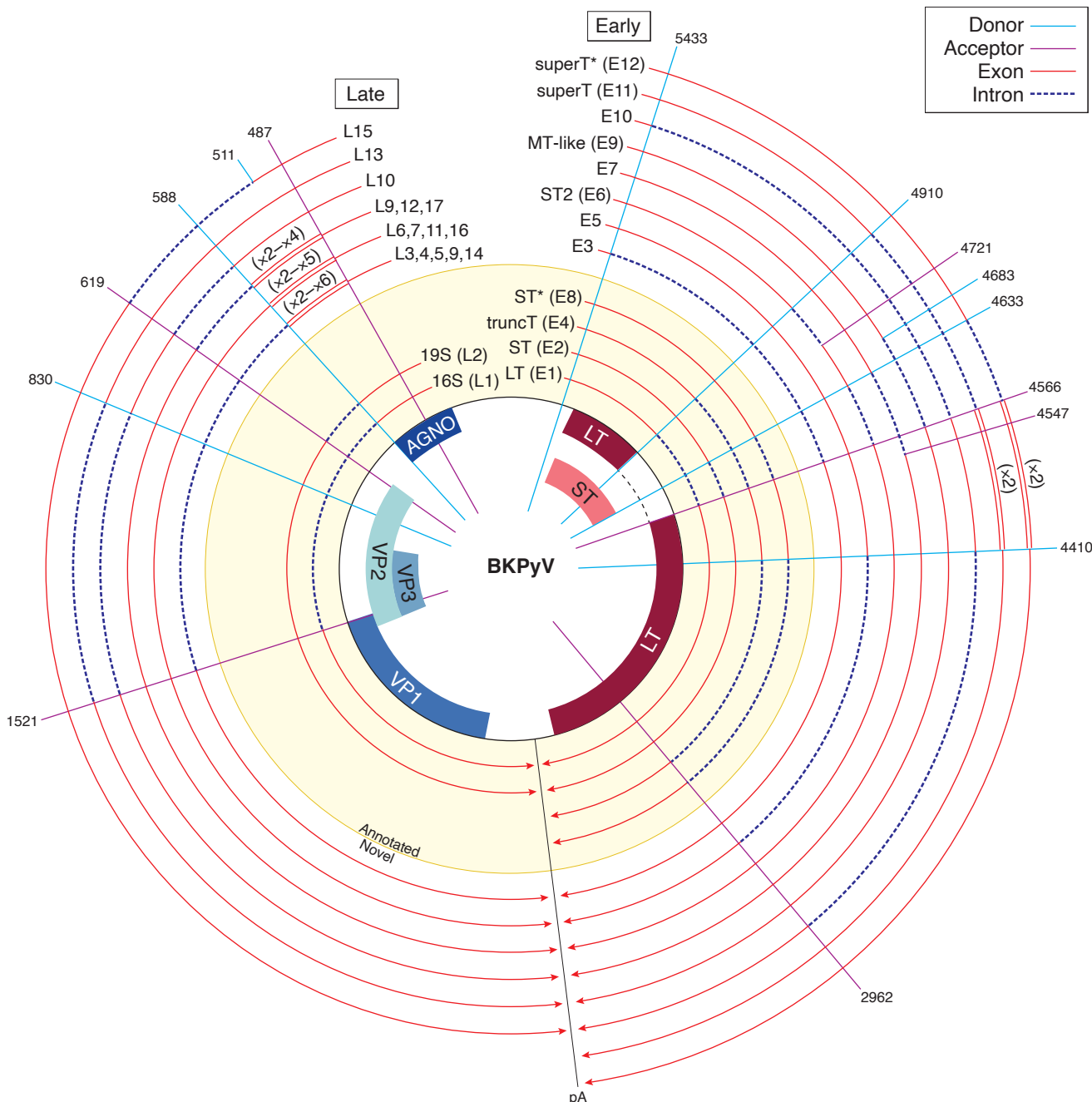
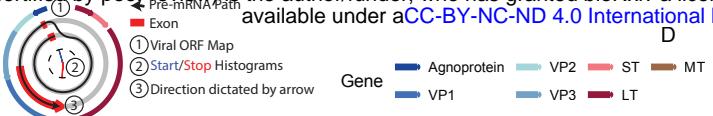


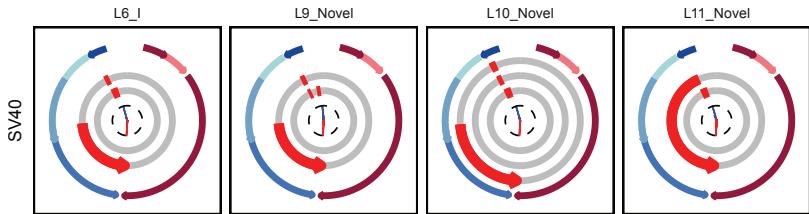
Figure 3 - Annotated and novel BKPyV transcripts.

A. Transcripts are shown relative to the viral genome. Each line is a viral transcript, with red lines indicating exons and dashed blue lines indicating introns. Spokes indicate the positions of common splice donors and splice acceptors. Transcripts that were annotated prior to this study are on a yellow background, and novel transcripts are on a white background. Wraparound transcription that results in multiple copies of a region is annotated with double lines, and the number of copies is indicated in parentheses. The line labeled "pA" indicates the approximate position of the polyA signal sequence.

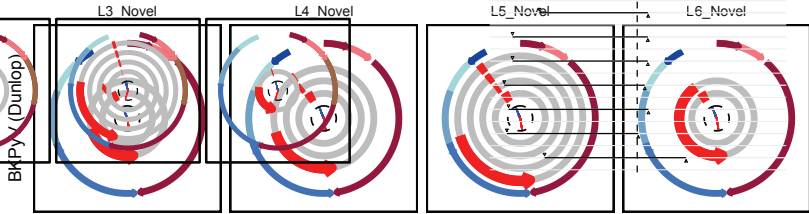
A



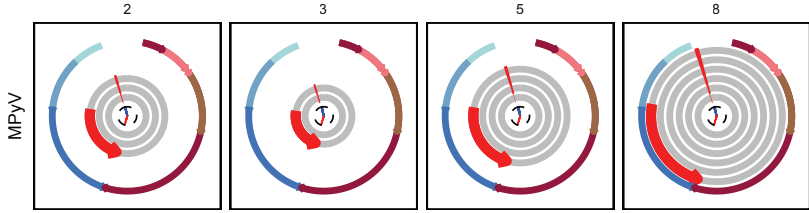
D



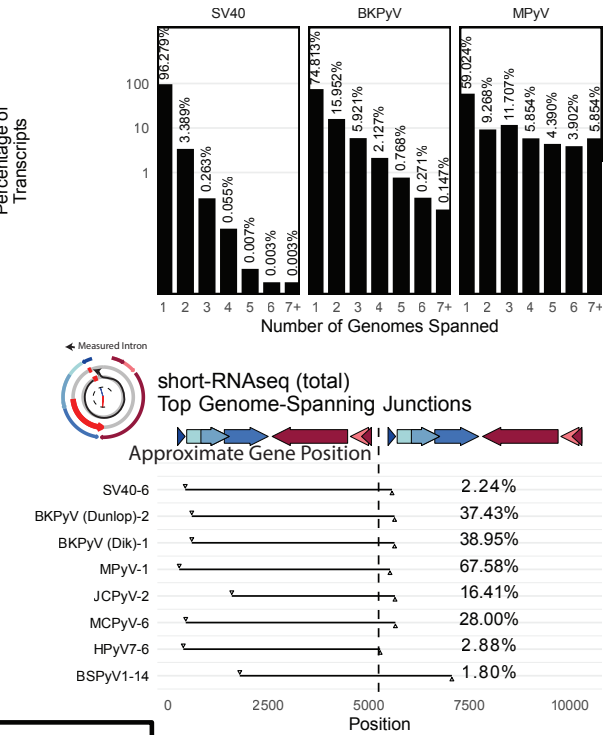
B



C



E



Transcript of origin
Short reads
Viral reference genome

F

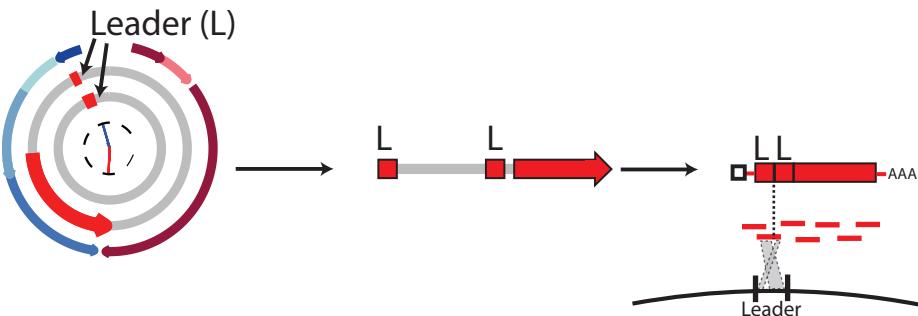


Figure 4 - Pervasive wraparound transcription across PyV

A-C. Watch plots indicating the top 4 highest abundance late wraparound transcript classes in dRNAseq data from SV40 (A), BKPyV Dunlop (B), and MPyV (C). The outer ring of each watch plot indicates the position of the viral ORFs. The inner arms are histograms detailing the distribution of transcript starts (in blue) and ends (in red) for transcripts within each transcript class. The red segments indicate exons. Transcripts start in the innermost ring - a second or third ring indicates that the pre-mRNA that generated the transcript must have circled the viral genome multiple times. The 3' end of the transcript and the direction in which these plots are oriented is indicated by the red arrow at the end of the last exon segment. The red exon segments start at the most common transcript start site within the transcript class, and end at the most common transcript end site within the class. The watch plot key shows an example of the path of the pre-mRNA for SV40 transcript class L6_I.

D. Bar plots indicating the percentage of late transcripts that span a given number of genome lengths in SV40, BKPyV Dunlop, and MPyV dRNAseq data.

E. The leader-leader junction, that connects the pre-mRNA from one genome to the subsequent wraparound, was identified in Illumina short-RNAseq (total) data. The intron in question is plotted as a black line in this plot, with the x axis indicating the genomic position of the intron. The top late wraparound transcript for each virus was plotted. The gene map indicates the approximate gene position and is accurate for SV40 - the exact position of the viral genes varies between viruses. Percentages indicate the percentage of late junction-spanning transcripts that support the plotted wraparound leader-leader junction.

F. Schematic illustrating how leader-leader wraparound transcription can be detected from short read short-RNAseq (total). Leader-leader splicing can be seen as a repetitive exon in watch plots from long-read RNAseq data. Ultimately, there was an original processed mRNA in the cell that contained two tandem leader sequences. When this transcript of origin is sequenced via short read sequencing, reads will be generated across its length. A minority of these reads will span the leader-leader junction, and mapping against the viral reference genome can be used to uncover leader-leader splicing.

Figure 5

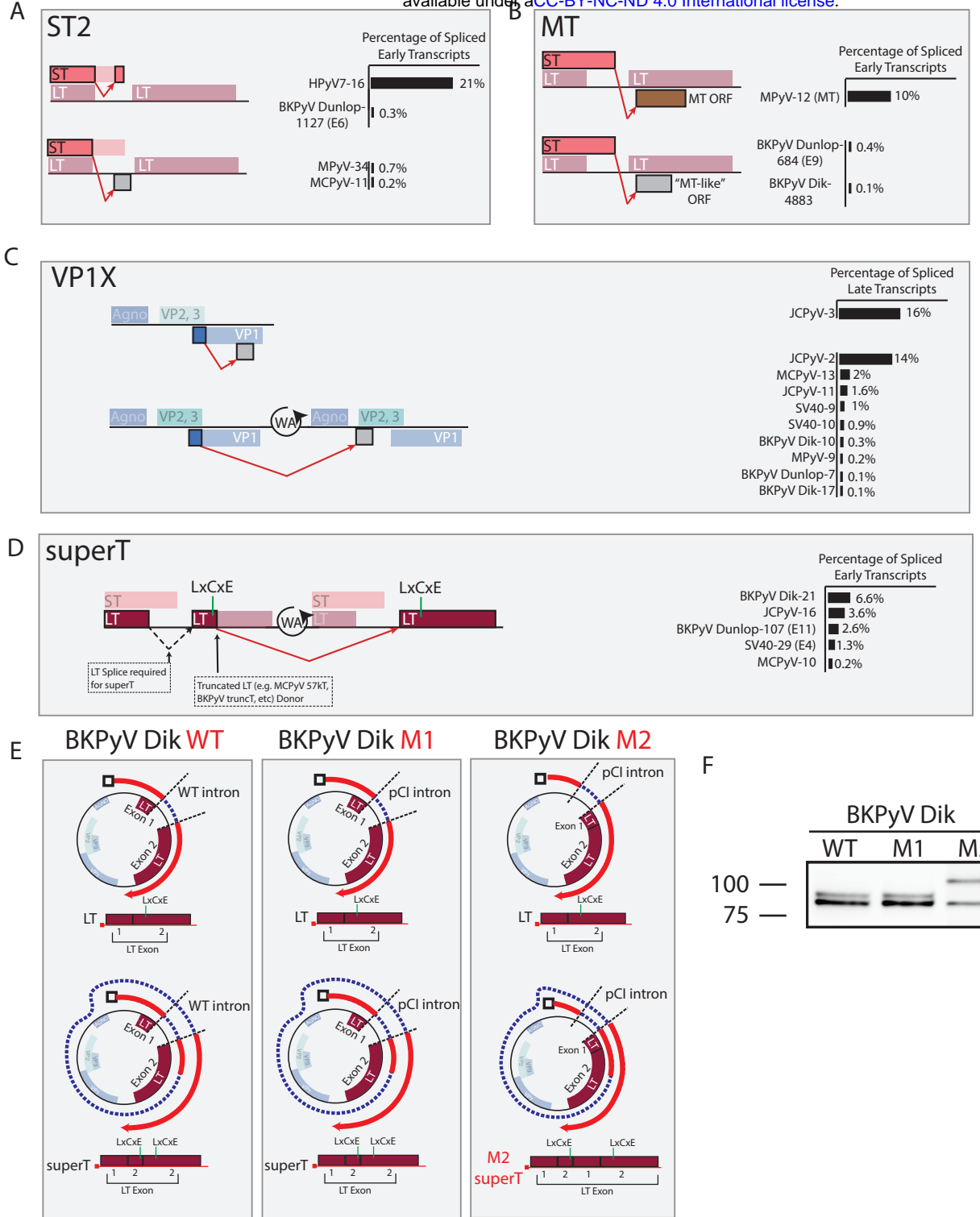


Figure 5 - Detection of novel, conserved splicing events that expand PyV coding capacity.

A-D. Schematics illustrating identified ORFs. Each row is a reading frame (except for ST and the LT 1st exon, which are in the same frame), and unannotated amino acids are represented by grey boxes. The measured intron is indicated by the red arrow. Colored ORFs are annotated, while grey ORFs are unannotated. Percentages on the right side of the figure are the percentage of spliced viral transcripts on the same strand as determined from short-read short-RNAseq (total) data. Numbers after each virus name indicate the transcript class within each short-RNAseq (total) dataset. The measured intron is indicated by the red arrow.

A) ST2: This ORF is generating from a splicing event that uses the LT first exon donor and an acceptor within the ST ORF. In HPyV7 and BKPyV Dunlop, the splice lands in frame and results in an internal deletion within ST. In MPyV and MCPyV the splice lands out of frame, resulting in an ORF that contains the N-terminal region of ST and novel amino acids at the C terminus.

B) MT: MPyV encodes a MT following splicing connecting the end of the ST ORF with an ORF in an alternate frame of the LT second exon. In BKPyV, a similar splice occurs connecting ST with an MT-like ORF in an alternative frame of the LT second exon.

C) VP1X: JCPyV encodes two VP1X ORFs generated by splicing within VP1 and landing in an alternative frame of VP1, or earlier in the late region due to wraparound transcription. While predominant in JCPyV, VP1X is likewise present in many other PyV.

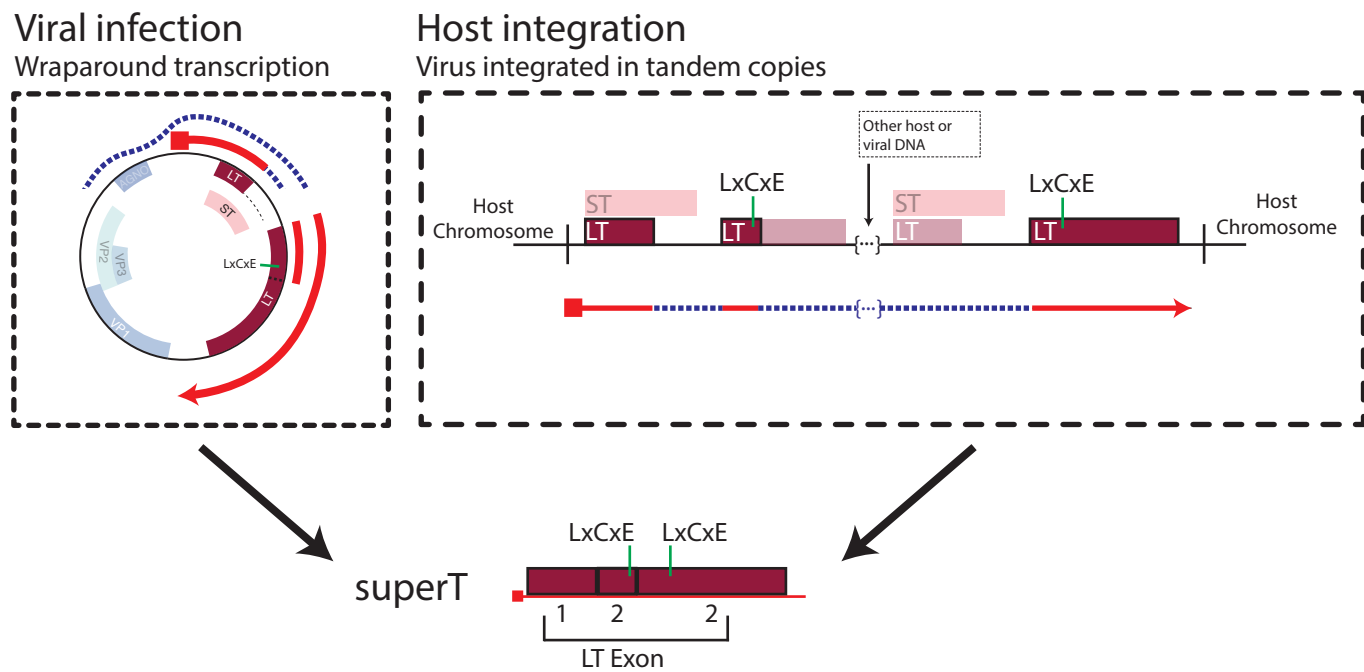
D) superT: The superT-specific splice utilizes the splice donor canonically associated with truncated T antigens such as 17kT in SV40 and truncT in BKPyV. Due to wraparound transcription, a LT second exon acceptor is available to the 3' of this donor and acts as the acceptor. For the superT ORF to form, an initial LT splice is required. Ultimately, superT contains a duplication in part of the LT second exon that includes the RB-binding LxCxE motif.

E. Schematics detailing BKPyV Dik isolates used for querying the existence of superT. BKPyV WT is wild type virus. M1 contains a LT intron that has been replaced with an intron from the plasmid pCl. Both WT and M1 are expected to generate LT and superT of expected sizes. M2 has a completely removed LT intron, and the pCl intron is located directly 5' of the LT ORF. M2 is expected to encode LT of expected size, but a larger superT variant due to incorporation of a second copy of the LT first exon.

F. Western blot of cells infected with BKPyV Dik WT, M1, or M2 and probed with an antibody reactive against LT. The lower molecular weight band is LT, and the higher molecular weight bands are consistent with superT.

Figure 6

A



B

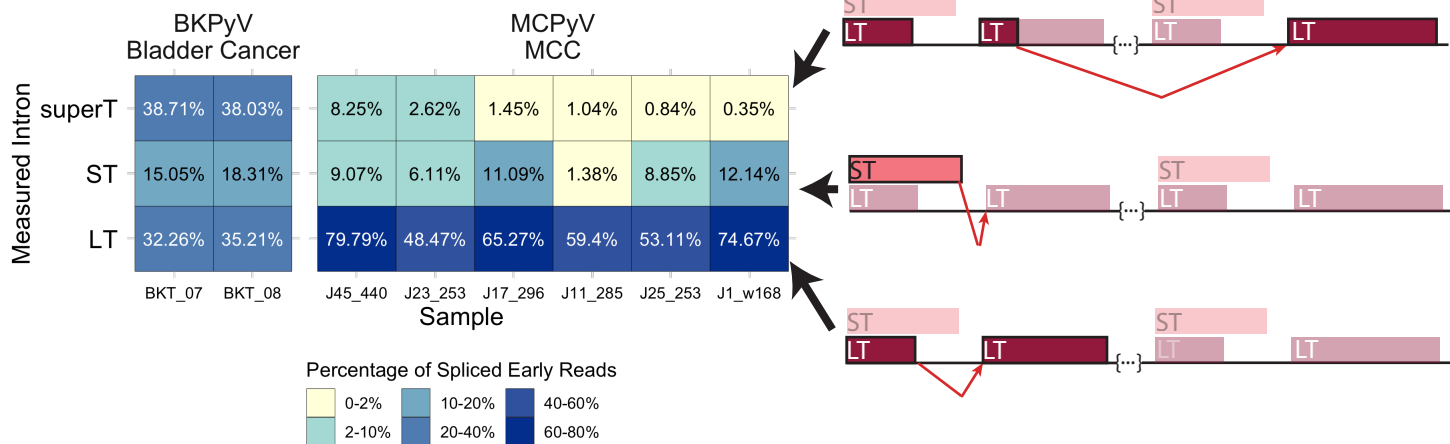


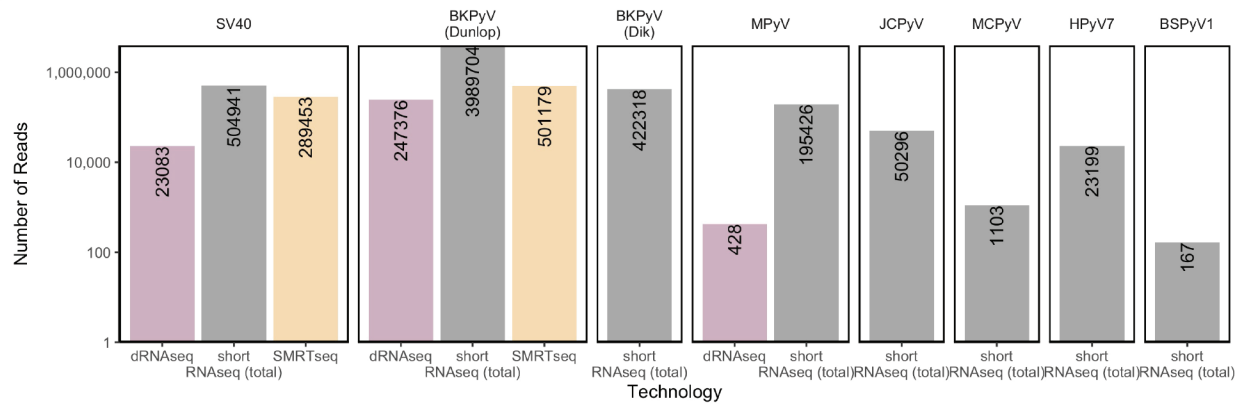
Figure 6 - Detection superT-encoding transcripts in PyV-associated cancers

A. Schematic detailing the generation of superT during lytic infection as compared to from integrated virus in cancer. During viral infection, the RNA polymerase can circle the viral genome multiple times, resulting in a pre-mRNA that can be spliced to generate superT. In the case of host integration, a polyomavirus can be integrated in tandem copies such that a pre-mRNA is generated with more than one copy of the viral early region. This pre-mRNA can be similarly spliced to generate a superT transcript.

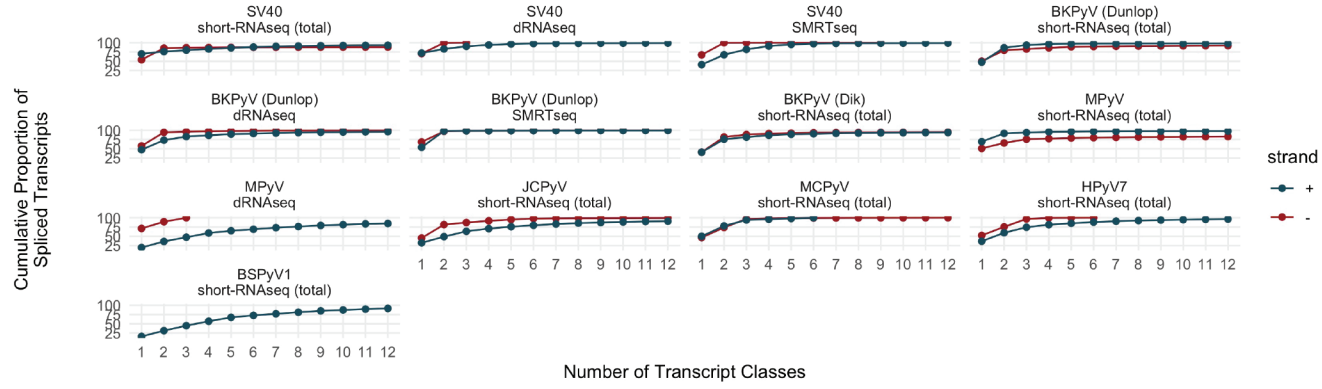
B. Heatmap indicating the abundance of the superT, ST, and LT introns from RNAseq data from two replicates of a BKPyV-positive bladder cancer and six MCPyV-associated MCCs. Percentages indicate the percentage of spliced early viral reads for each sample. The splice measured in each row is indicated by the red arrow in the schematics on the right side of the figure.

Fig S1

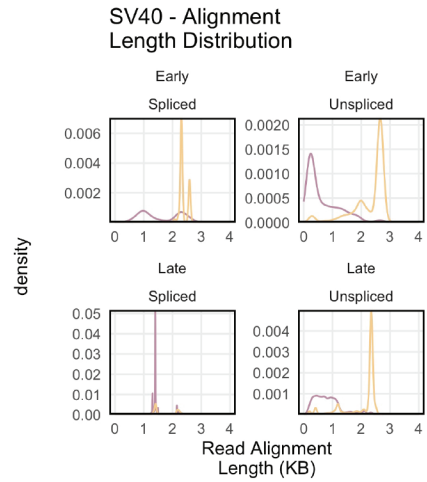
A



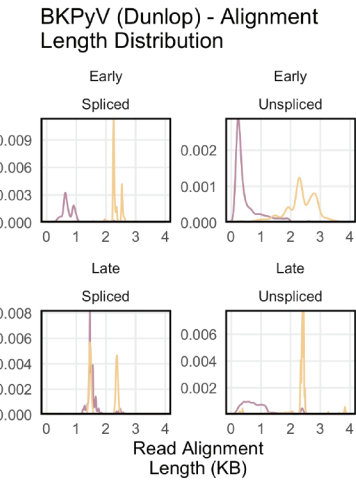
B



C



D



E

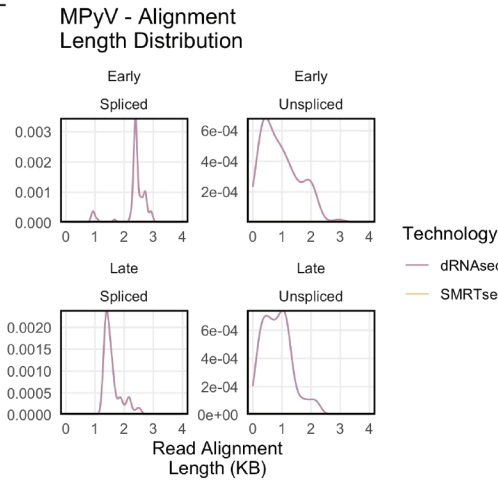
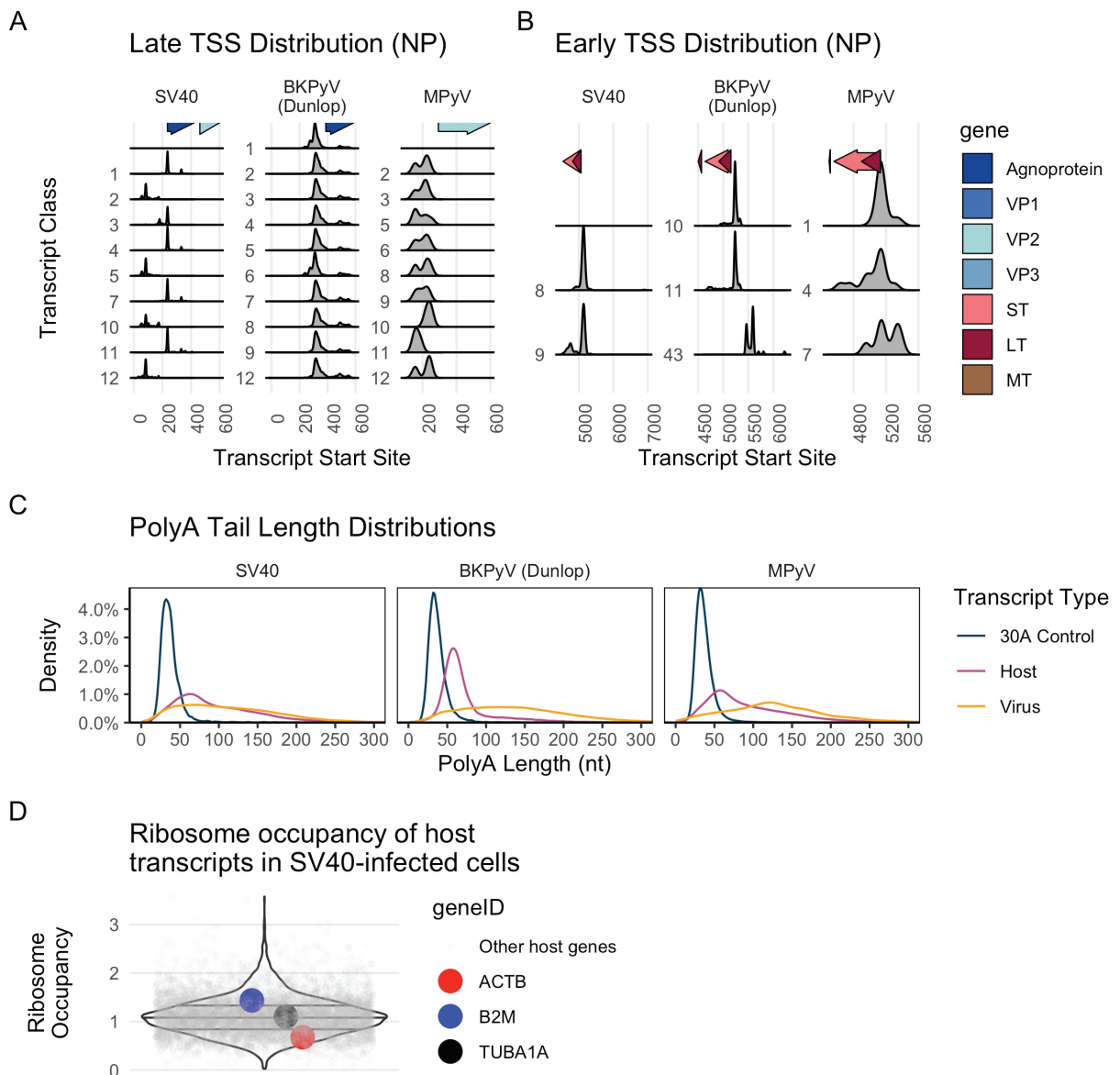
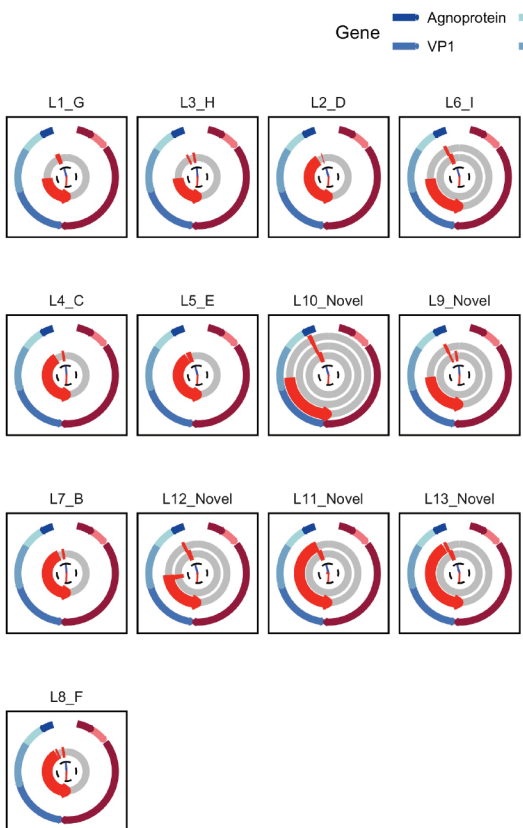


Figure S2

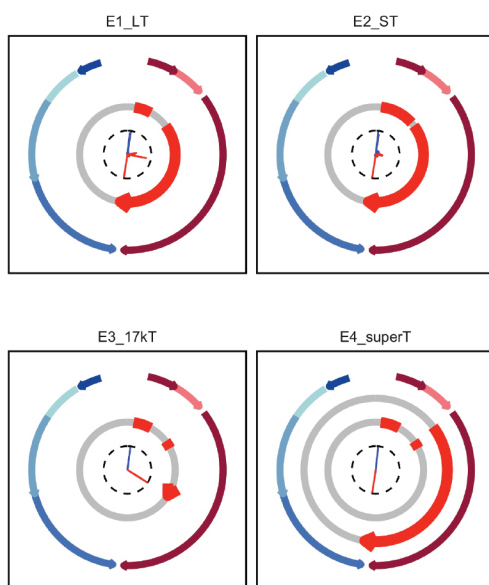


FigS3: SV40 Transcriptome

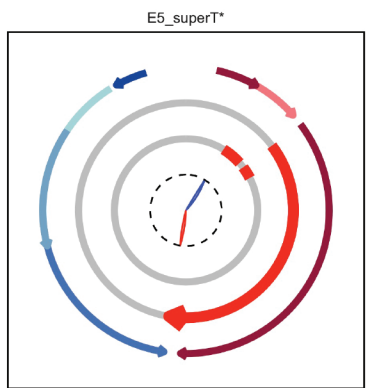
A SV40: dRNAseq + SMRTseq, Late



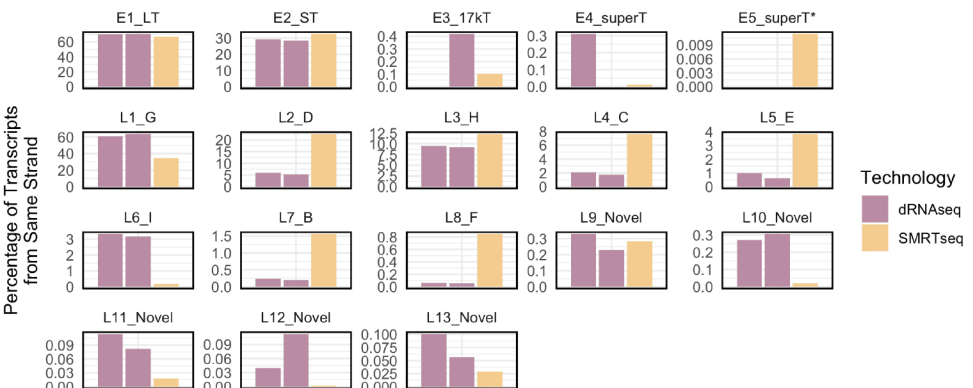
B SV40: dRNAseq + SMRTseq, Early



C SV40: SMRTseq Only

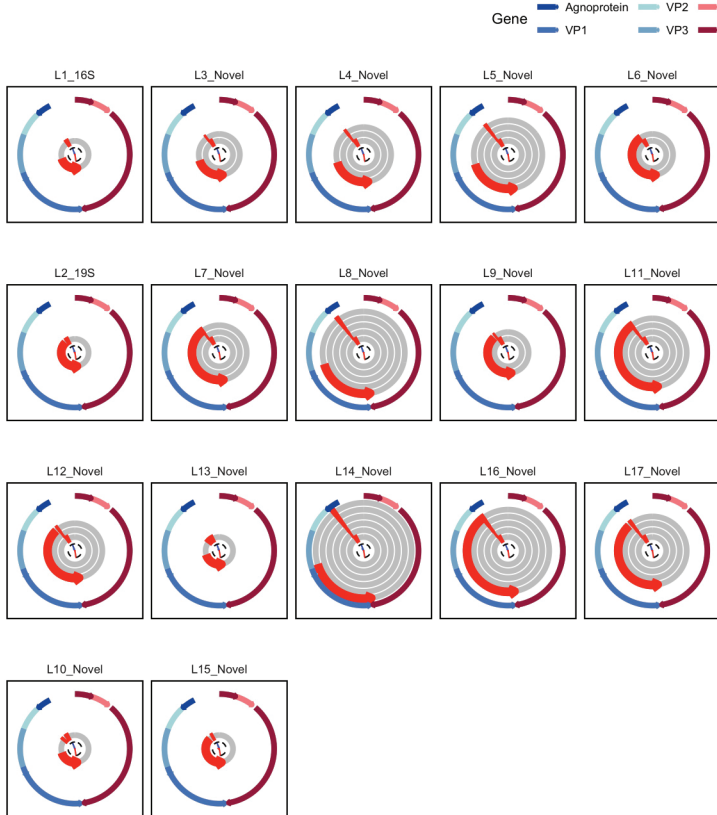


D

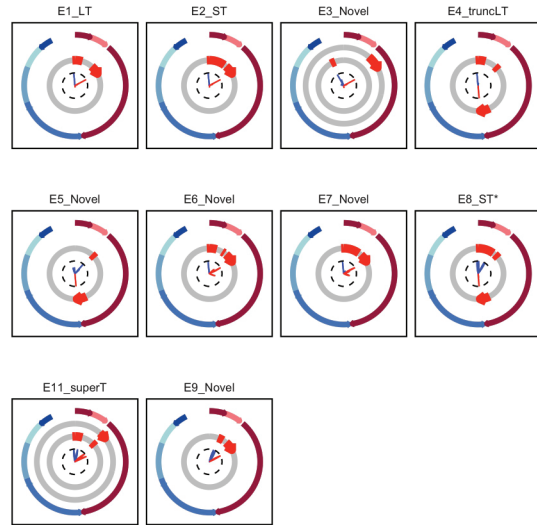


FigS4: BKPyV (Dunlop) Transcriptome

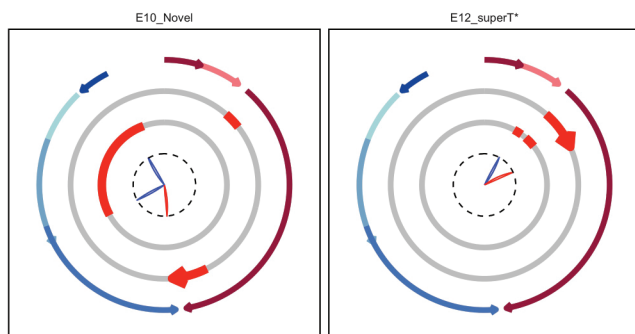
A BKPyV (Dunlop): dRNAseq + SMRTseq, Late



B BKPyV (Dunlop): dRNAseq + SMRTseq, Early



C BKPyV (Dunlop): dRNAseq Only



D

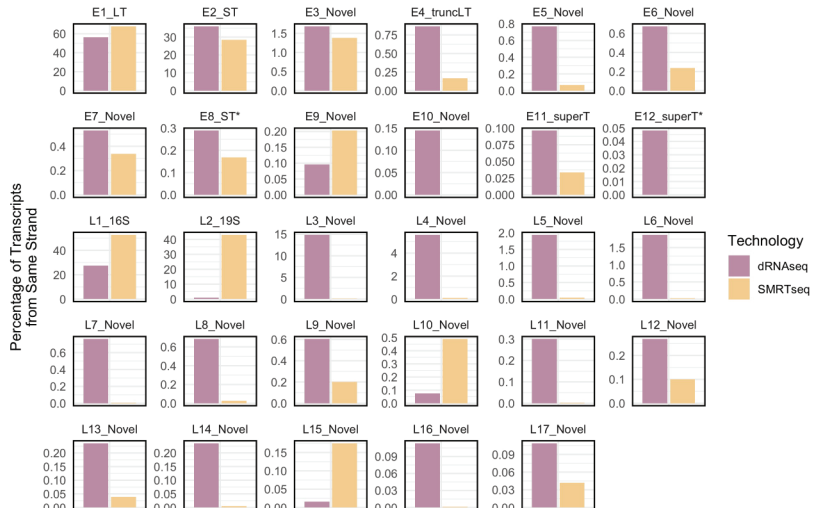
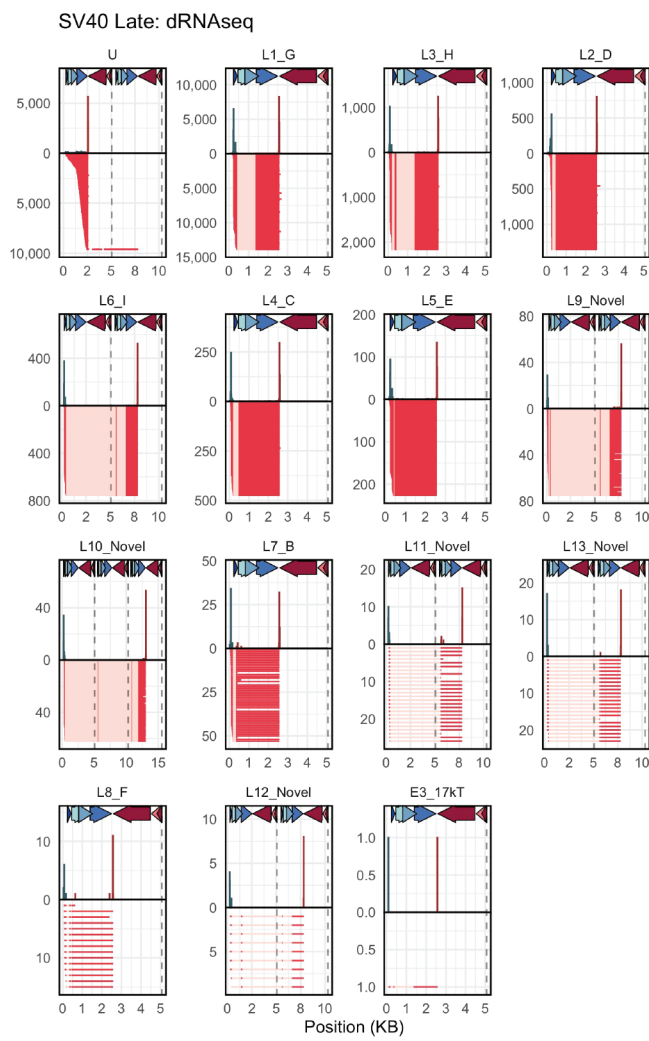
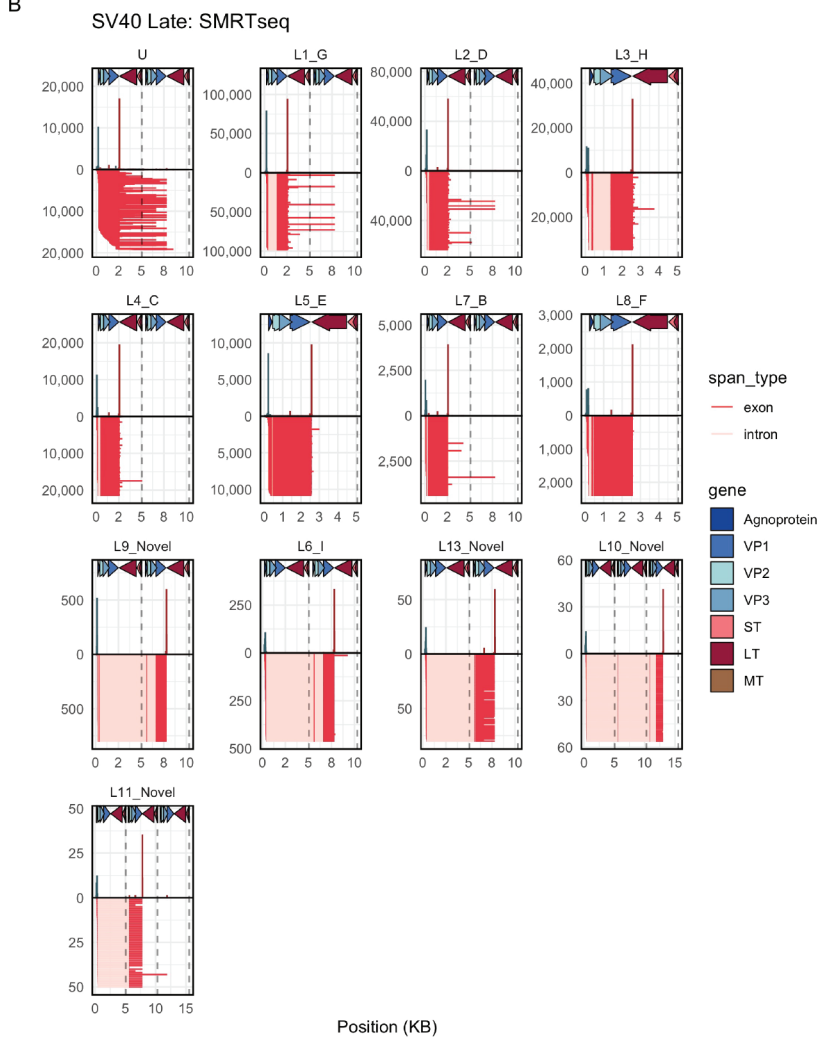


Fig S5: SV40 Late Transcript Pileups

A



B



span_type

- exon
- intron

gene

- Agnoprotein
- VP1
- VP2
- VP3
- ST
- LT
- MT

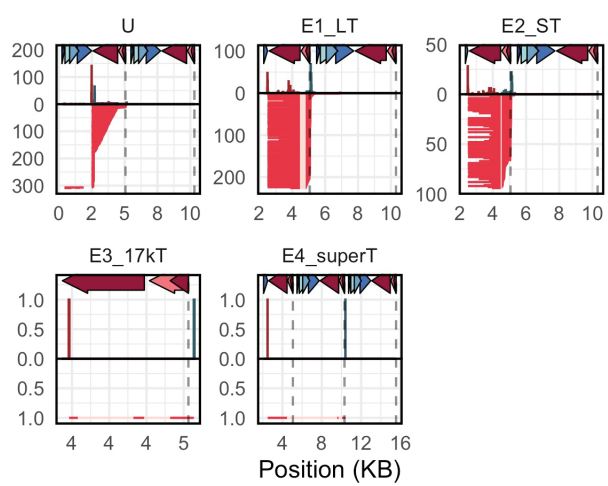
Position (KB)

Position (KB)

Fig S6: SV40 Early Transcript Pileups

A

SV40 Early: dRNAseq



B

SV40 Early: SMRTseq

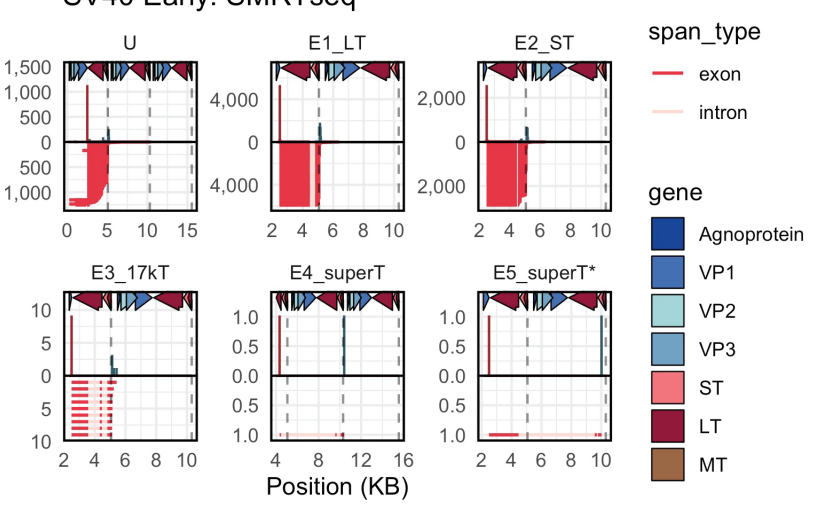
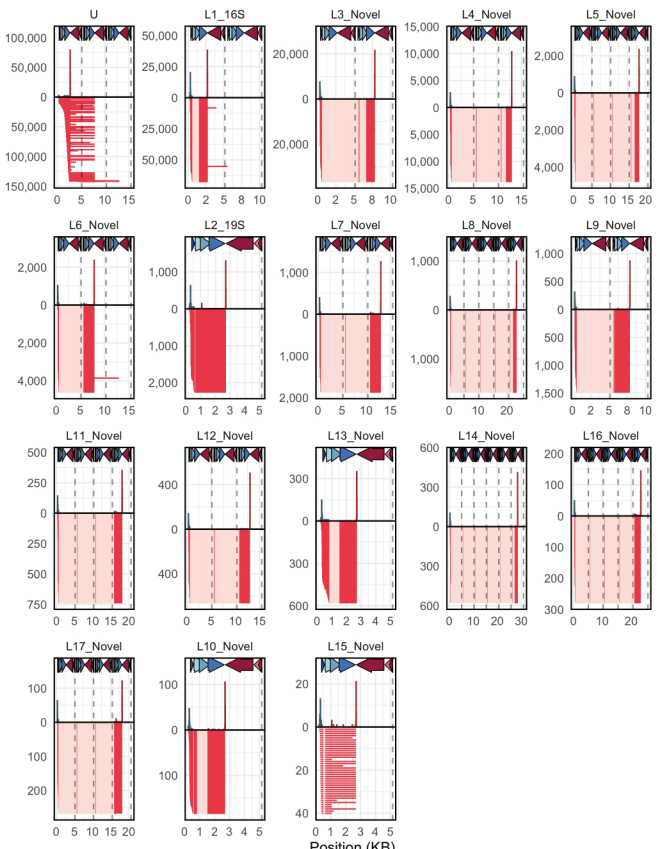


Fig S7: BKPyV (Dunlop) Late Transcript Pileups

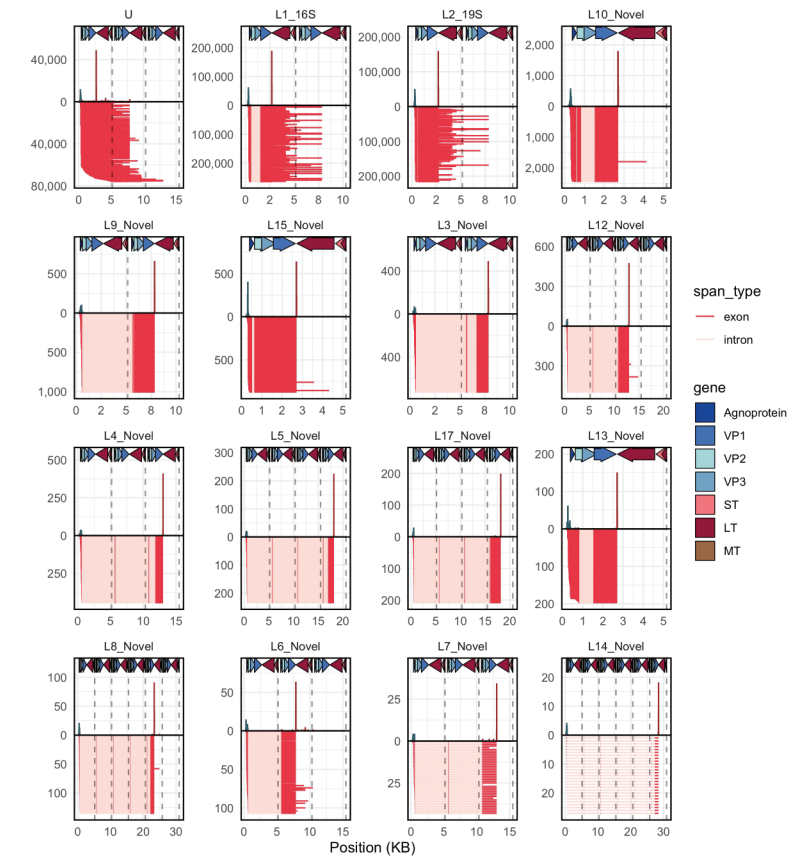
A

BKPyV (Dunlop) Late: dRNAseq



B

BKPyV (Dunlop) Late: SMRTseq



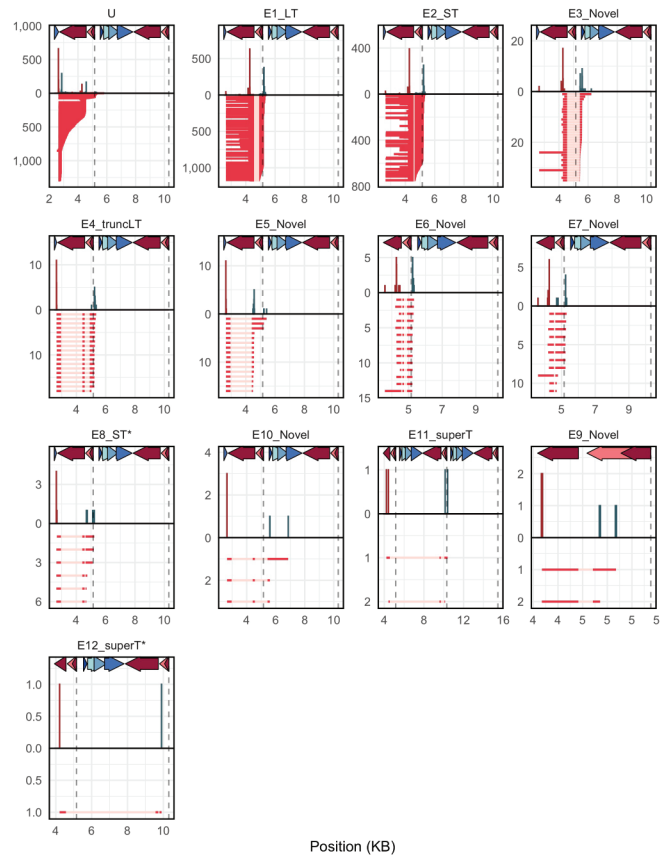
span_type
exon
intron

gene
Agnoprotein
VP1
VP2
VP3
ST
LT
MT

Fig S8: BKPyV (Dunlop) Early Transcript Pileups

A

BKPyV (Dunlop) Early: dRNAseq



B

BKPyV (Dunlop) Early: SMRTseq

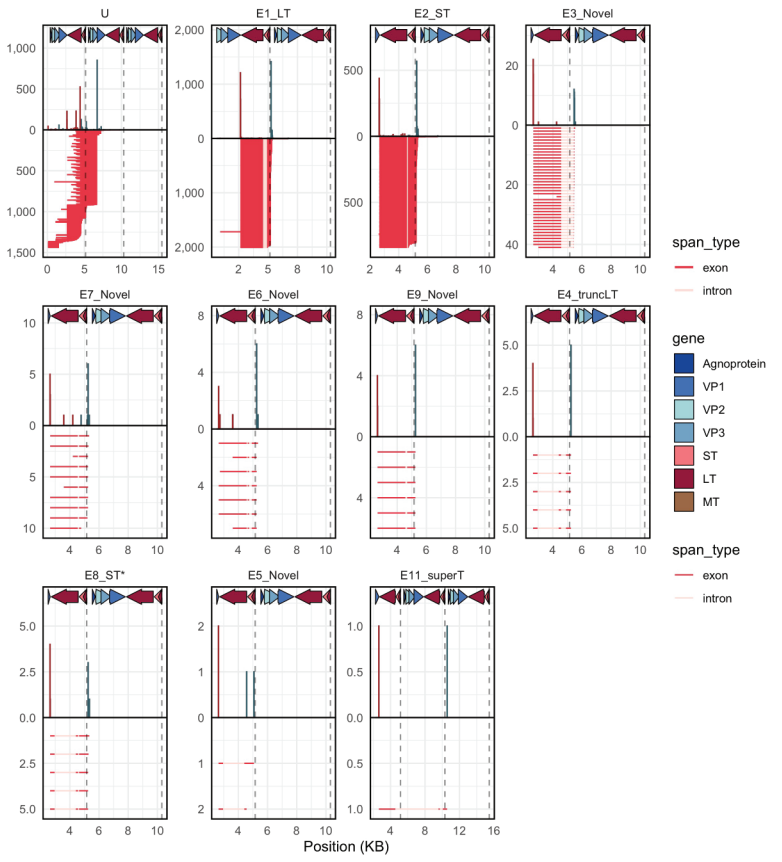
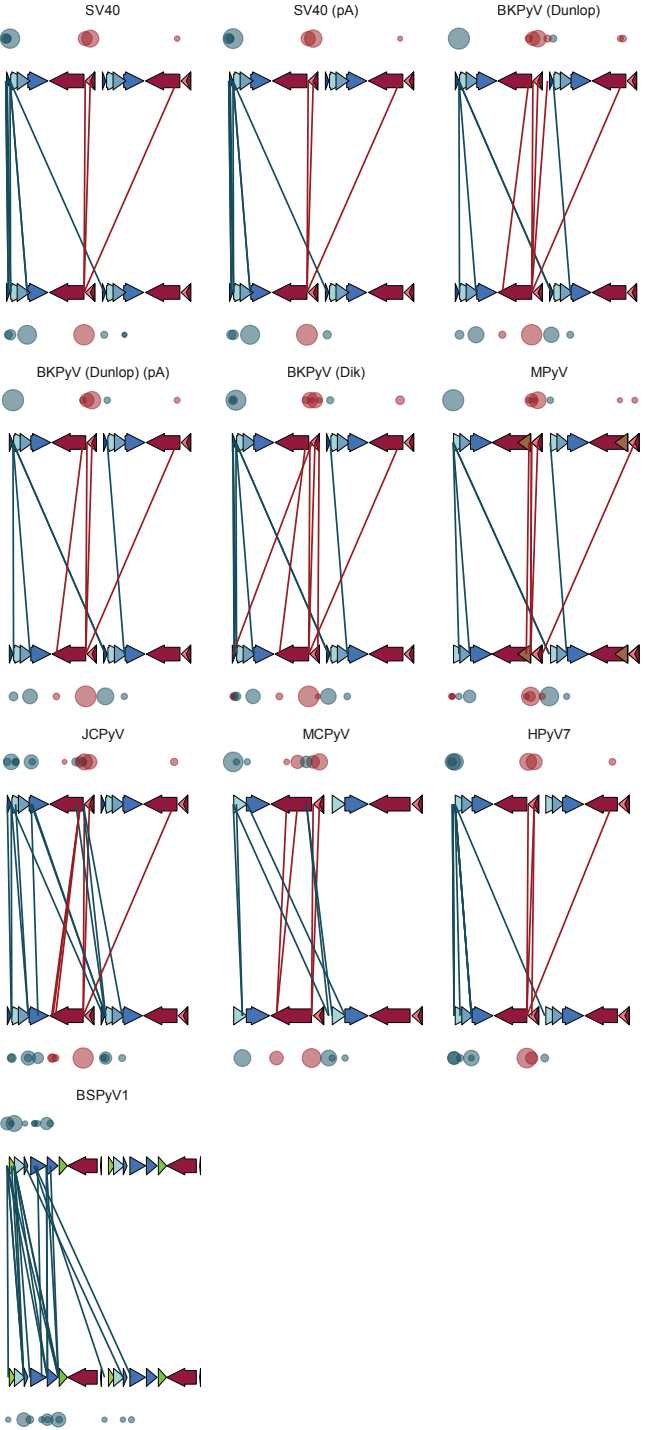


Fig S9

Illumina Introns >1% of Junction-spanning reads (by strand)

available under aCC-BY-NC-ND 4.0 International license.

A



B

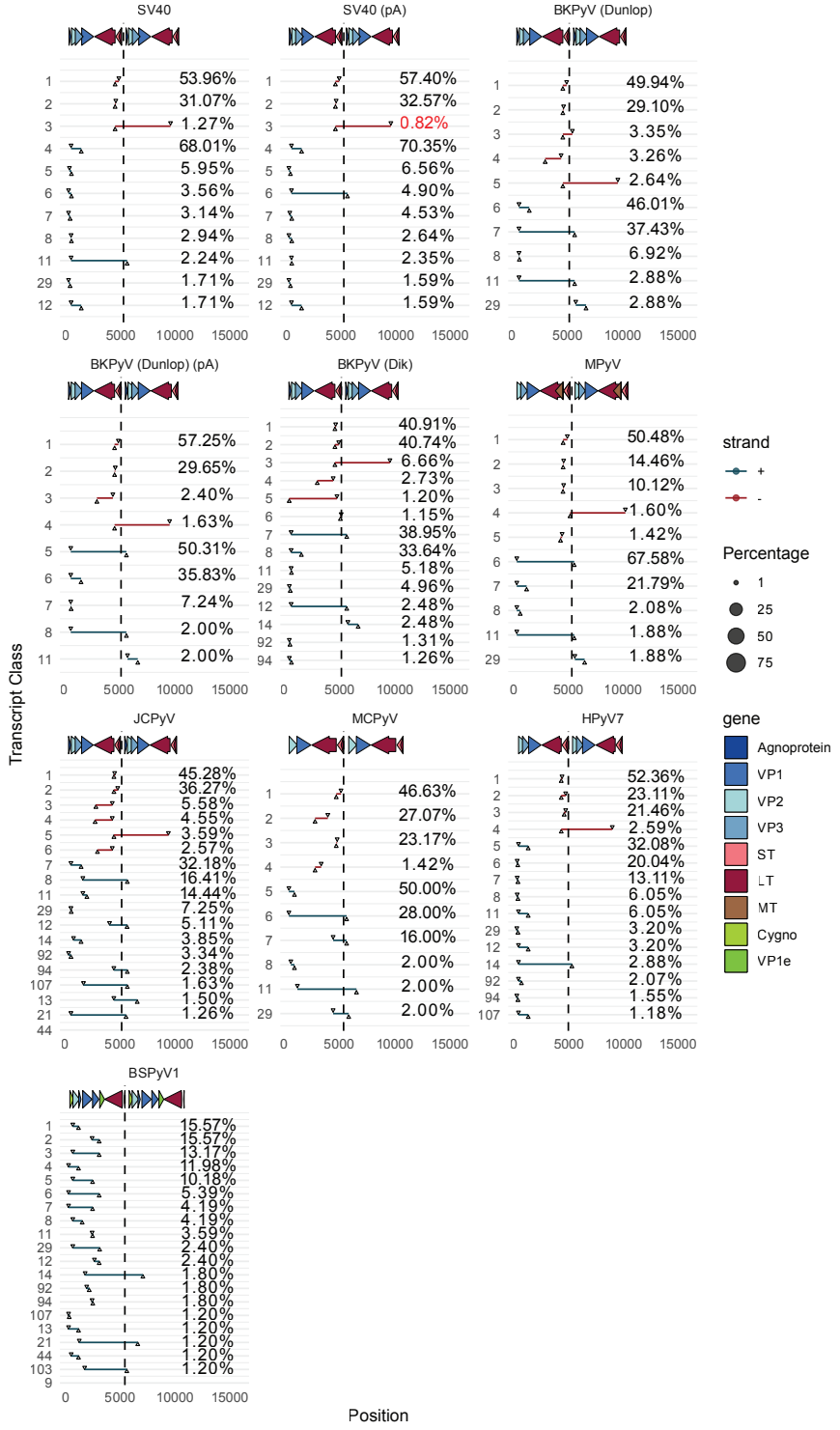


Figure S10

A

LT and ST Transcripts
Watch Plots

D

Alternative Polyadenylation of
Early Spliced Transcripts

E

LT and ST
Transcripts
PolyA Lengths

B

E1_LT E2_ST

BKPyV (Dunlop)

C

LT (NP Class 1) ST (NP Class 4)

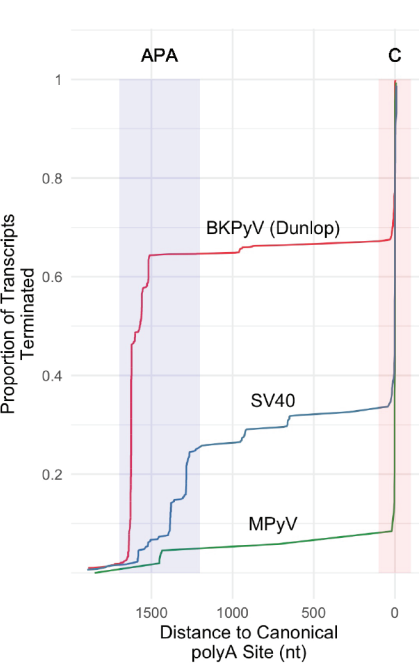
MPyV

Gene

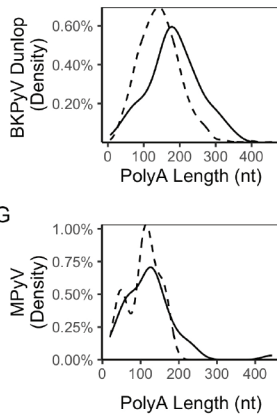
- Agnoprotein
- VP2
- ST
- MT
- VP1
- VP3
- LT

Transcript Status

- APA
- Canonical



F



G

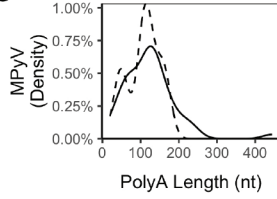
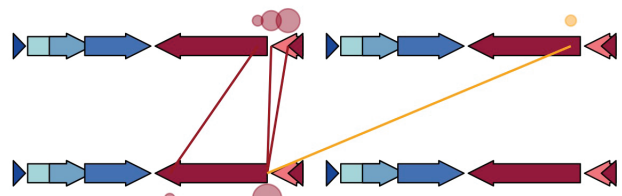


Fig S11

BKPyV Dik short-RNaseq (polyA)

A

BKPyV Dik WT (pA)

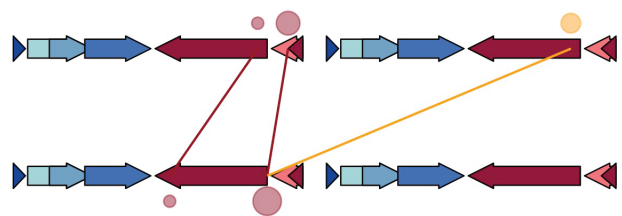


Percentage

- 1
- 25
- 50
- 75

B

BKPyV Dik M1 (pA)

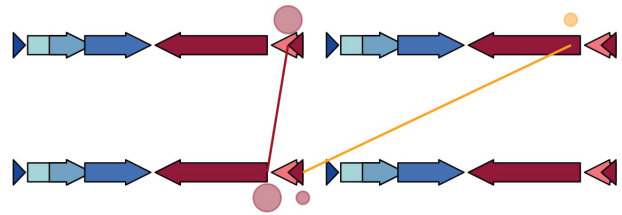


gene

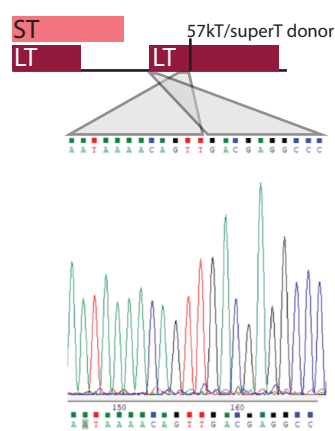
- Agnoprotein
- VP1
- VP2
- VP3
- ST
- LT

C

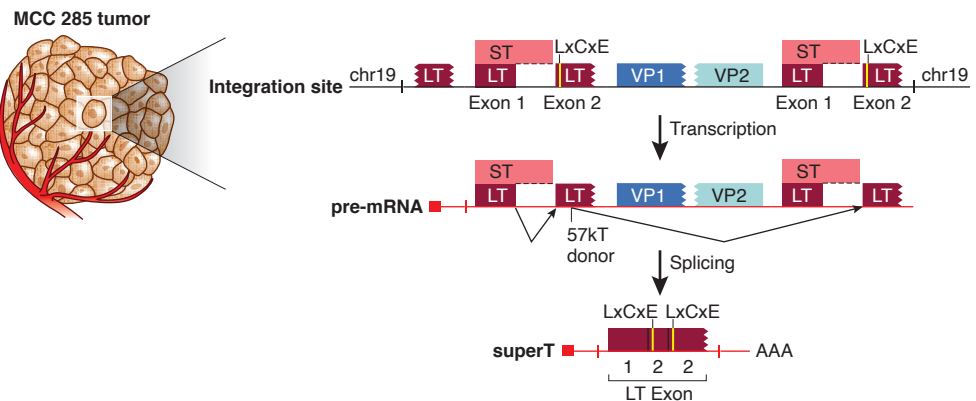
BKPyV Dik M2 (pA)



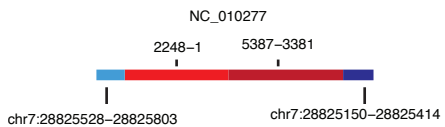
A Tumor: J45_440



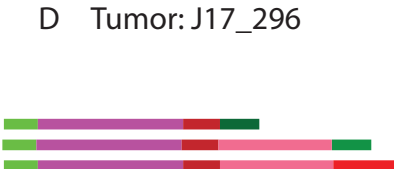
B



C Tumor: J45_440



D Tumor: J17_296



- chr2:174708385-174708543
- chr2:174844338-174844520
- chr2:174844524-174844754
- NC_010277_2_revComp_NCCR_TAg:1-429
- NC_010277_2_revComp_NCCR_TAg:1691-2994
- NC_010277_2_revComp_NCCR_TAg:2980-5387
- NC_010277_2_revComp_NCCR_TAg:415-1705

